Distortion modeling and Machining of aerospace materials

by

ABBAS HUSSAIN

A Thesis Submitted to the

Graduate School of Engineering

in Partial Fulfillment of the Requirements for

the Degree of

Doctor of Philosophy

in

Mechanical Engineering

Koc University

August 2019

Koc University

Graduate School of Sciences and Engineering

This is to certify that I have examined this copy of a doctoral thesis by

ABBAS HUSSAIN

and have found that it is complete and satisfactory in all respects,

and that any and all revisions required by the final

examining committee have been made.

Committee Members:

____

Ismail Lazoğlu, Ph. D. (Advisor)

____

Erdem Alaca, Ph. D.

____

Üğur Ünal, Ph. D.

____

Seyed Ehsan Layegh Khavidaki, Ph. D.

____

Armin Bijanzad, Ph. D.

Date: 07.08.2019

To My

Teachers

parents

wife

daughter

brothers

&

friends

ABSTRACT

Milling process is used in the machining of advanced engineering materials such as Gamma Titanium Aluminide, Titanium and Aluminum Alloys. These materials have various aerospace applications, such as 48-2-2 Gamma Titanium Aluminide and Ti-6Al-4V due to their superior thermo-mechanical properties are used in the aircraft engines and rockets. Whereas, Al7050 is mainly utilized in aircraft structural parts. The aircraft parts are consisting of thin-wall structures and often suffer a deformation which causes a dimensional surface error due to the action of the mechanical and thermal loads generated during the milling process. Therefore, the deformation of thin-walled structural parts is the major problem in aerospace industries. This problem may lead to low productivity, part rejection and high production cost. To avoid part rejection and achieve better machining results it becomes necessary to predict the distortion of the part before going into actual machining.

In this thesis, a 3D transient finite element based model is developed to predict the distortion of the Al7050 thin-wall complex structural parts due to the milling process. The combined effect of mechanical and thermal load is considered in the model. These loads are analytically estimated and used as an input for the FEM simulation. A new approach is proposed for applying the mechanical and thermal loads on the final part geometry. Milling experiments in 5-axis CNC machining center are performed in order to validate the simulation results. The results are validated using force measurements, temperature measurements, laser measurements, and coordinate machine measurements.

Besides the distortion modeling, machining tests on Gamma Titanium Aluminide (γ-TiAl) and Ti6Al4V Alloys are performed. The novelty of the study lies in reporting the orthogonal database of 48-2-2 γ-TiAl. The developed database is used to predict the cutting forces for milling process for Ti-48Al-2Cr-2Nb (48-2-2) γ-TiAl by employing orthogonal to oblique transformation technique. High-performance coatings have become a successful standard for increasing the efficiency of machining tools in industry over the last decade. The study focuses on establishing an orthogonal cutting database for different tool coatings; AlTiN and AlCrN coatings. The effect of coating on friction coefficient, shear stress, shear angle and cutting forces are investigated. Friction coefficient identified from the orthogonal turning shows that the AlCrN coating has the highest friction coefficient as compared to the AlTiN coating whereas the AlCrN coating has a smaller shear angle as compared to the AlTiN coating. Predicted cutting forces are validated with the experimental cutting forces during end milling and ball-end milling operations for different cutting conditions. The simulated results showed good agreement with the experimental results. Overall, this study provides an important guide for machining of 48 2-2 γ-TiAl alloys and facilitating the transition from processing traditional materials to advanced materials for manufacturing industries.

ÖZET

Frezeleme işlemi Gama Titanyum Alüminid, Titanyum ve Alüminyum alaşımları gibi ileri mühendislik malzemelerinin işlenmesinde kullanılır. Bu malzemeler, özellikle 48-2-2 Gamma Titanyum Alüminid ve Ti-6Al-4V, üstün termo-mekanik özelliklere sahip oldukları için uçak motorları ve roketler gibi çeşitli havacılık uygulamalarında kullanılır. Al7050 ise temel olarak uçakların yapısal parçalarında kullanılmaktadır. İnce cidarlı uçak parçaları, frezeleme işlemi sırasında ortaya çıkan mekanik ve termal yüklerin etkisiyle boyutsal bir yüzey hatasına neden olan deformasyona uğrarlar. Bu nedenle, ince cidarlı yapısal parçaların işlenme sonucunda oluşan deformasyonu, havacılık endüstrisindeki en büyük problemlerdendir. Bu sorun düşük üretim verimliliğine, parça reddine ve yüksek üretim maliyetine yol açabilir. Parça reddini önlemek ve daha iyi parça işleme sonuçları elde etmek için, parça işlemeye başlamadan önce parçaların boyutsal bozulmasının öngörülmesi gerekir.

Bu tezde, ince cidarlı ve karmaşık geometriye sahip Al7050 yapı parçalarının frezeleme işleminden kaynaklanan boyutsal bozulmaları tahmin etmek için bir 3D geçici sonlu eleman tabanlı model geliştirilmiştir. Mekanik ve termal yükün birleşik etkisi modelde göz önünde bulundurulmuştur. Bu yükler analitik olarak tahmin edilmiş ve sonlu elemanlar simülasyonu için bir girdi olarak kullanılmıştır. Mekanik ve termal yüklerin son parça geometrisine uygulanması için yeni bir yaklaşım önerilmiştir. Simülasyon sonuçlarını doğrulamak için 5 eksenli CNC işleme tezgahında frezeleme deneyleri gerçekleştirilmiştir. Simülasyon sonuçları kuvvet ölçümleri, sıcaklık ölçümleri, lazer ölçümleri ve koordinat makinesi ölçümleri ile deneysel olarak doğrulanmıştır.

Boyutsal bozulmanın modellemesinin yanı sıra, Gamma Titanyum Alüminid (γ-TiAl) ve Ti6Al4V alaşımları üzerinde de işleme testleri yapılmıştır. Bu çalışma ile daha önce literatürde olmayan 48-2-2 γ-TiAl malzemesi için bir ortogonal kesim veri tabanı

oluşturulmuştur. Ortogonal kesimden eğik kesime dönüşüm tekniği kullanılarak geliştirilen veri tabanı, Ti-48Al-2Cr-2Nb (48-2-2) γ-TiAl malzemesinin frezeleme işlemindeki kesme kuvvetlerini tahmin etmek için kullanılır. Yüksek performanslı kaplamalar, son on yılda, endüstrideki işleme takımlarının verimliliğini artırmak için başarılı bir standart haline gelmiştir. Bu çalışma AlTiN ve AlCrN takım kaplamaları için ortogonal kesim veri tabanı oluşturmaya da odaklanmaktadır. Kaplamanın sürtünme katsayısı, kayma gerilmesi, kayma açısı ve kesme kuvvetleri üzerindeki etkisi incelenmiştir. Ortogonal tornalama işlemi ile bulunan sürtünme katsayıları değerlendirildiğinde, AlCrN kaplamanın AlTiN kaplamasına kıyasla daha yüksek sürtünme katsayısına sahip olduğunu, ancak AlCrN kaplamanın AlTiN kaplamasına göre daha küçük bir kayma açısına sahip olduğunu görülmüştür. Öngörülen kesme kuvvetleri, uç freze ve bilyeli freze takımları kullanılarak farklı kesim koşulları için yapılan deneylerden ölçülen kesme kuvvetleriyle karşılaştırılarak, doğrulanmıştır. Simüle edilen sonuçlar, deneysel sonuçlarla iyi bir uyum göstermiştir. Genel olarak, bu çalışma, 48 2-2 γ-TiAl alaşımlarının işlenmesi ve imalat sanayinde geleneksel malzemelerin işlenmesinden gelişmiş malzemelerin işlenmesine geçişi kolaylaştırmak için önemli bir rehber sunmaktadır.

ACKNOWLEDGEMENTS

Finishing this dissertation is a product of several years' work. There are many great people who have greatly inspired and supported me during my PhD.

First, I would like to thank my thesis supervisor Professor. Dr. Ismail Lazoglu for providing me the opportunity, the continued guidance, and support throughout the research period at the advance world-class facilities of the Manufacturing and Automation Research Center.

I would like to acknowledge the continuous support and prayers of my parents Hussain Ghulam Ali, Hawwa Hussain and my brother Qutbuddin Hussain, that encouraged me to go ahead in my study and career. And, I am most thankful to my wife Marium Abbas for believing in me and boost my confidence at the time when I needed it most. She had to continue and show tremendous courage in taking care of my daughter, while I was abroad. As to my little angel, Sarrah Abbas, my love for her are beyond words. I am most thankful to my daughter for giving me the first eight months of her life.

I would also like to thank the respected thesis review committee members, Assoc. Prof. Erdem Alaca and Assoc. Prof. Ugur Unal for their valuable time and input during the periodic committee meetings. I would also like to thank the respected thesis committee members for the review and input.

My special thanks to Dr. Seyed Ehsan Layegh Khavidaki, Dr. Mohammad Akmal, Dr. Talha Irfan Khan and Muzaffar Abi for the help and technical support in my Ph.D. studies. I also deeply appreciate MARC members especially Haris, Sarmad, Adnan, Shahid Mustafa, Hosain, Omer, Anjum, Çağlar, Abasin, Enes, Başar, Isa, Sheheryar, Atacan, Munem, Shams and mubin for their support.

On behalf of the MARC, I also would like to acknowledge the Scientific and Technological Research Council of Turkey (TUBITAK), Turkish Aerospace Industries (TAI), MANUNET and Karcan Cutting Tool Company, for their support.

I wish to thank the Higher Education Commission of Pakistan for funding my PhD studies abroad. I would like to thank Koç University for its efficient administration and high-quality support.

Finally, I express my gratitude to the great nation of Turkey in general, for giving me such beautiful memories, wonderful experience and amazing friends that will be unforgettable.

TABLE OF CONTENTS

LIST OF TABLES

LIST OF FIGURES

NOMENCLATURE

dF_t, dF_r, dF_a	Differential force components in tangential, radial and axial directions
dF_x, dF_y, dF_z	Differential force components in the X, Y and Z directions
F_x, F_y, F_z	Cutting force in the X, Y and Z directions
θ	Tool immersion angle
θ_{exit}	Cutter exit angle
R	Tool radius
j	Current tool flute number
N	Total tool flute number
z	Axial depth of cut
z_1	Lower engagement position of the cutter disk
z_2	upper engagement position of the cutter disk
h	Uncut chip thickness
d_z	Disk thickness in axial direction
a_e	Radial width of cut
K_{rc}, K_{tc}, K_{ac}	Cutting Force coefficients in radial, tangential and axial directions
K_{re}, K_{te}, K_{ae}	Edge Force coefficients in radial, tangential and axial directions
$\dot{Q}_s$	Shearing power
$\dot{Q}_f$	Friction power
$\dot{Q}_T$	Total heat generation rate
P_W	Fraction of heat flow into the workpiece
$\dot{Q}_W$	Heat flow into the workpiece
F_s	Shear force on shear plane
F_u	Friction force on rake face
F_R	Resultant cutting force

V_s	Shear velocity
V_c	Chip velocity
V	Cutting velocity
τ_s	Average shear flow stress
α_n	Normal rake angle
β_a	Friction angle
β_n	Normal friction angle
$\emptyset_n$	Normal shear angle
$\emptyset_c$	Shear angle
$d\varepsilon_{elastic}$	Elastic strain
$d\varepsilon_{plastic}$	Plastic strain
$d\varepsilon_{total}$	Total strain
ρ	Density
E	Modulus of elasticity
ν	Poisson’s ratio
λ	Thermal conductivity
S	Specific heat capacity
α	Coefficient of thermal expansion
E_w	Element width
E_l	Element width
E_h	Element height
D	Cutter tool diameter
n	Spindle speed
f	Feedrate
α_r	Rake angle
α_n	Normal rake angle

i	Inclination angle
η	Chip flow angle
F_{fc}	Average feed cutting force
F_{tc}	Average tangential cutting force
b	Width of cut in orthogonal cutting
r_c	Chip thickness ratio
$k(z)$	Tool axial immersion angle
$db(z)$	Chip width of cutting disk
$dS(z)$	Edge length of cutting disk
i_o	Helix angle

Chapter 1
INTRODUCTION

1.1 Overview

In today's modern and competitive world, industrial sectors required manufactured parts with high productivity and quality while achieving the required surface qualities and reducing the production costs. In this regard, the aerospace industry is the most stringent in safety regulation for parts integrity and reliability. The capability to simulate and control the manufacturing process of intended parts is a keenly sought objective. According to the "International Air Transport Association (IATA) survey" [1], the global passenger numbers are forecast to double to 8.2 billion by 2037 and it will create 119 million jobs. Based on this report, it can say that the aerospace industry is flourishing and is facing an increasing demand of high quality machined parts.

The milling process is one of the main process utilized in aerospace manufacturing. The parts are commonly manufactured using aluminum alloys, shown in Figure 1-1. The advantage of using aluminum is that it provides low cost, lightweight solution for the manufacturer and the parts are easy to manufacture as compared to the other high-performance materials. Al7050 was developed during the 1970s and due to its lightweight, greater corrosion resistance and strength, efficiency it is the premier choice for aerospace application [2]. Especially in the aerospace industry, the complex thin-wall structural parts are manufactured by the milling process in which up to 90% of the material is removed, shown in Figure 1-2. Due to the material removal process, shearing and friction phenomena occurs which causes the mechanical and thermal loads, and therefore the final shape of the part deviates from the original design, shown in Figure 1-3. These distorted parts can require extra time and efforts for the corrections after the machining. Therefore, due to the milling induced distortions, an increase in the production costs become inevitable and, in some cases, excessive distortions may lead to rejection of the expensive aerospace parts. Distortion in thin-wall parts can range from a few micrometers to several millimeters depending on the dimensional scale of the part and utilized machining parameters. According to the study, the distortion of the parts due to heat treatment and machining cost the US Boeing company around $290 million lost in four projects, while it cost Germany about 850 million euros lost [1].

Figure 1-1: Use of aluminum alloy in aircraft components [2]

Figure 1-2: Machining of large aerospace monolithic parts [3]

Figure 1-3: Deformed airframe part [4]

In order to improve the engine performances and efficiency in the aircraft, as well as to satisfy the increasingly restrictive environmental regulations, aimed at reaching a decisive lessening of CO_2 emissions, the advancement in the structural material has been made by introducing the new lightweight structural materials with superior thermo-mechanical properties [5]. In this context, intermetallic aero-engine materials, such as γ-TiAl, have been identified as strategically critical materials to be used in both non-rotating and rotating components, e.g. blade manufacturing. They provide a remarkable strength-to-weight ratio, approximately half the density of nickel-based superalloys, high stiffness, high elastic modulus, strength retention at elevated temperatures, oxidation resistance, and good creep properties [8,9]. It took more than 20 years of very intensive research to obtain maturity level of TiAl-based alloys that is enough to consider this class of materials for critical rotating components in commercial jet engines [10]. However, the attractive mechanical and thermal properties, become a drawback when dealing with machining, as it occurs with many other materials. As it has been shown in several conventional machining publications, machinability of γ-TiAl is poor because of its low ductility combined with high hardness and brittleness at room temperature, low thermal conductivity, low fracture toughness and chemical reactivity with many tool materials. In consequence, the machining cost is high, which can restrict the widespread use of these materials in the industry.

1.2 Thesis Outline

The research presented in this dissertation is organized as follows: A detailed literature review on distortion modeling and machining of aerospace material γ-TiAl is provided in Chapter 2. A 3D-finite element modeling approach is presented in Chapter 3 for the prediction of distortion in complex thin-wall structural parts. A combined effect of mechanical and thermal load is considered, and a new approach is proposed to apply the thermo-mechanical load in the model. Experiments are performed and the model is validated with online and offline distortion measurement. In Chapter 4, the machining of 48-2-2 γ-TiAl is performed. An orthogonal database is developed for 48-2-2 γ-TiAl for two different coating conditions. Using the developed database and analytical force model, the cutting forces are predicted for end mill and ball-end milling operations. Estimated results are validated through sets of experiments for different cutting conditions.

Chapter 2
LITERATURE REVIEW

2.1 Overview

This chapter presents a detailed literature review on the different aspects linked to the aviation industry and is organized as follows:

The chapter has seven sections in which the first section provides the structure of this literature review. In the second section, a brief introduction on conventional machining processes and more specifically the milling process and the advancement in CNC milling technology is realized. The third section provides the history, uses, and advantages of different aerospace materials used in this dissertation. Then in the fourth section, the previous research work realized on cutting force model for orthogonal cutting and oblique cutting (milling operation) is studied. Different thermal models to predict the temperature of tool, chip and workpiece in milling operation are presented in the fifth section. The sixth section aims to review the previous work related to the machining induced part distortion. Different models used to predict the machined part quality are presented. Finally, In the seventh section, previous studies related to the machining of gamma titanium aluminide more specifically the milling of gamma titanium aluminide is realized.

2.2 Machining Processes

Machining is a very common and useful subtractive manufacturing method. It can be classified into conventional or traditional machining and non-conventional machining.

In conventional machining, a cutting tool is used to remove the unwanted material from the workpiece in order to get the final desired shape. It can be categories into the following processes:

- Single-point cutting processes
  - The turning
  - The planning and shaping
- Multi-point cutting processes
  - The milling
  - The drilling
  - The broaching
  - The sawing
- Abrasive cutting processes
  - The grinding
  - The honing
  - The lapping
  - The ultrasonic machining
  - The abrasive jet machining

Non-conventional machining processes utilize chemical or thermal means to remove the material. It can be listed as follows:

- Chemical cutting
  - The chemical machining
  - The electrochemical machining (ECM)

- Thermal
  - The torch cutting
  - The electrical discharge machining (EDM)
  - The high energy beam machining

The selection of the machining process is dependent on the part geometry, desired accuracy, and surface quality. In this thesis, both orthogonal turning and milling experiments are performed.

The turning operation is the metal cutting operation used to manufacture cylindrical parts. In this process, the workpiece is attached to the rotating spindle while the cutter (single point cutting tool) is secured in the machine. The tool feeds into the rotating workpiece, cutting away material. In orthogonal turning, the cutting edge of the tool is perpendicular to the direction of the cutting velocity, shown in Figure 2-1(a).

In the aviation industry, the milling operation is most often utilized in the machining of aerospace aluminum alloy parts. The milling operation is the machining process in which the rotating cutting tool is used to remove the material from the workpiece. The workpiece is usually moved against the tool, however, in some cases, the workpiece is fixed, and the rotating tool is moved against it. Unlike turning, which is a continuous cutting operation, milling is an interrupted machining operation. During the milling operation, the cutting edges repeatedly enter and exit the engagement domain. From simple to complex geometries, the milling process allows the machining of parts with high accuracy. The geometry of the milling tool and the mechanics of the process is illustrated in Figure 2-1(b).

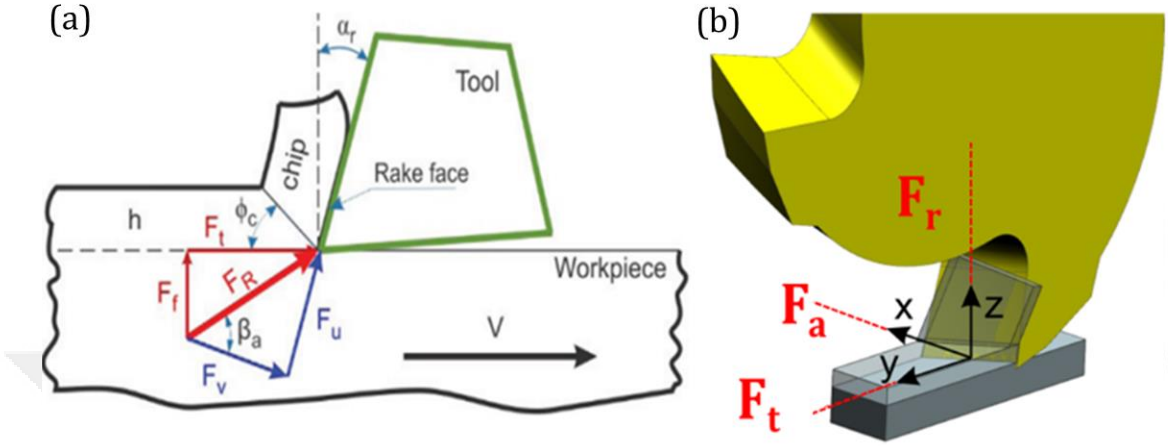

Figure 2-1: (a) Geometry of orthogonal turning operation, (b) Geometry of milling operation.

Development of the Computer Numeric Control (CNC) technology revolutionize the machining industry. The first milling machine was developed in the 18th century and after that, the technology was continued to be evolved. In this regard, the significant contribution occurred during the period 1949-1951with the development of the first control system at Massachusetts Institute of Technology (MIT). The early to mid-1970s was a period of advancement in the machining with the development of the computerized numerical control. In this period the CNC become reality and it gave industry the ability to change the workpiece geometry and manufacture the product with minimum time [6]. Over the years the CNC technology has come a long way. Today's CNC machines are well developed with the capabilities of multi-axis control, high speed machining, and multi-process manufacture allowing milling, turning and drilling operations on a single machine in one part setup [7]. The advantage of CNC technology is that it provides the manufacturing of the part with more flexibility and shorter production time. It allows the machining of micro-to-macro sized complex geometries for various materials [8]. In the progress of CNC technology, Computer Assisted Design/Manufacturing (CAD/CAM) software products also played an important role. These software programs allow to automatically generate tool paths and machining programs for complex geometries machining operations [9]. Currently, virtual machining is the area of interest in this field. The virtual machining provides the digital model for the manufacturing process which includes the conceptual design, engineering analysis and physics of the manufacturing process. The concept of virtual machining is illustrated in Figure 2-2

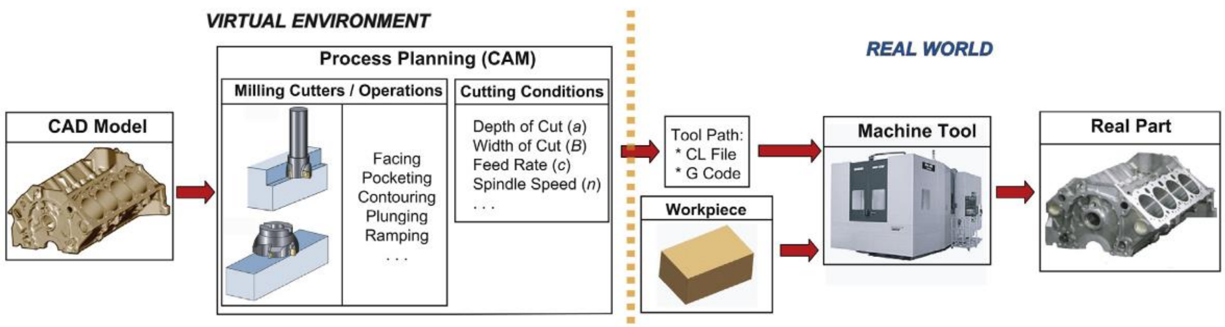

Figure 2-2: Virtual machining system architect [10].

Today CNC machining is commonly used in the industry, especially in the aerospace industry, the large complex parts are manufactured in five-axis milling machine center. The machining performance depends on workpiece material, tool path, operation sequence and cutting parameters. In the current research thesis, five-axis CNC milling machine center is utilized to perform the experiments for distortion modeling and machining of aerospace materials.

.

2.3 Aerospace materials

2.3.1 Aluminum alloys

Owing to low cost and lightweight metal, aluminum is one of the most easily fabricated of the high-performance materials. Significant improvement in aluminum alloys have occurred since they were first introduced in the 1920s, shown in Figure 2-3. Elements like copper, zinc, magnesium, iron, etc. are added to aluminum to give primary aluminum new mechanical properties [11]. Aluminum alloys are classified into workable alloys and cast alloys. The workable alloys are those which undergo the hot or cold mechanical working process, whereas the final shape is obtained by the casting process in the cast alloys. Table 2-1 demonstrates the series of workable aluminum alloys. Out of these series 2XXX, 7XXX and 6XXX are mainly used in aircraft construction [12]. Aluminum Alloys can be machined rapidly and economically.

Aluminum 7050 was developed during the 1970s and it belongs to 7XXX series of workable aluminum alloys. It is a heat treatable alloy, known as a commercial aerospace alloy. Owing to its strong mechanical strength, high fatigue strength and high resistance to stress corrosion cracking, the material is used to build fuselage frames, wing skins and other aerospace structures [13]. In this dissertation, heat treated Al7050 T7451 is used for the distortion experiment in Chapter 3.

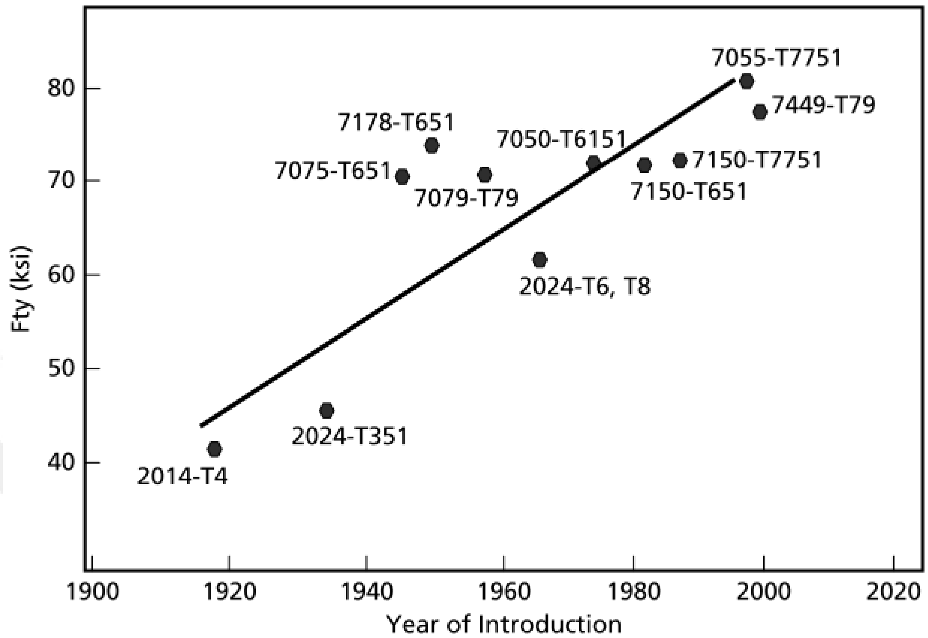

Figure 2-3: Yield strengths of aluminum alloys with respect to year of introduction[14]

Table 2-1: Designation of workable aluminum alloys [15]

Series	Main alloying elements
1XXX	Commercially pure aluminum >99 % purity
2XXX	Copper
3XXX	Manganese
4XXX	Silicon
5XXX	Magnesium
6XXX	Magnesium and Silicon
7XXX	Zinc
8XXX	Other elements e.g. lithium
9XXX	Not used

2.3.2 Titanium alloys

Titanium alloys are widely used in hi-tech industries. The attractive properties of titanium alloys with excellent corrosion resistance and strength efficiency makes it an important material for aerospace and power generation industry [16]. Ti-6Al-4V is the biocompatible material and are also commonly used in surgical implants of various kinds such as heart implants, bone implants and joint, etc.

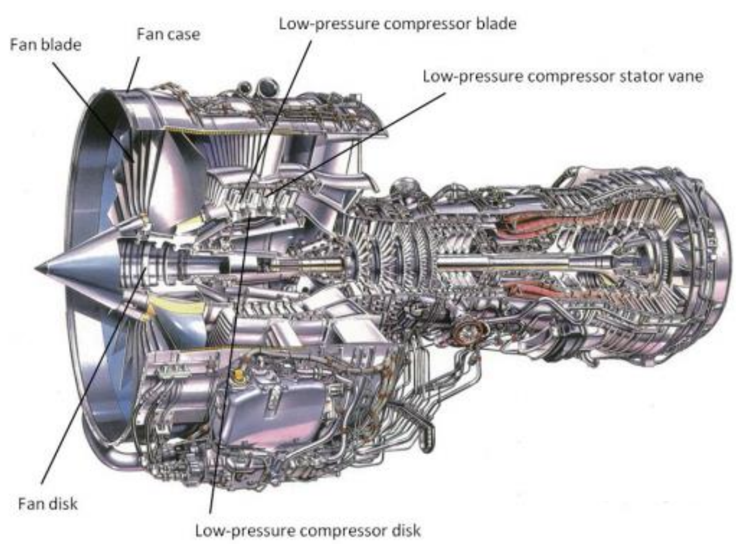

Figure 2-4: Application of Ti-6Al-4V in aero-engine V2500 [17].

Ti-6Al-4V has excellent mechanical strength, fracture toughness and corrosion resistance at high elevated temperature with low density and high strength efficiency. However, the low thermal conductivity and chemical reactivity make it hard-to machine material [18]. Despite the significant amount of published research and being used in the industry for over 50 years, the machining of titanium alloys remains a major concern, especially in terms of tool life and workpiece integrity [19].

2.3.3 Gamma titanium alloys

The advancement in technology put the effort towards the development of new materials. The path followed in this development is to introduce material to reduce the weight of the component and enhance its performance at a higher temperature. As an example, the overall efficiency of the turbine is highly dependent on the operating temperature and the thrust to weight ratio of the material used.

In this regard, the intermetallic compounds have attracted great interest since the first Materials Research Society symposium 1984 [20]. These compounds are formed by the interaction of two or more metallic elements to form a metallic bond. Silicides, beryllides and the aluminides are the some of the intermetallic. Among these titanium aluminides have the attractive properties to operate at higher temperature with lower density.

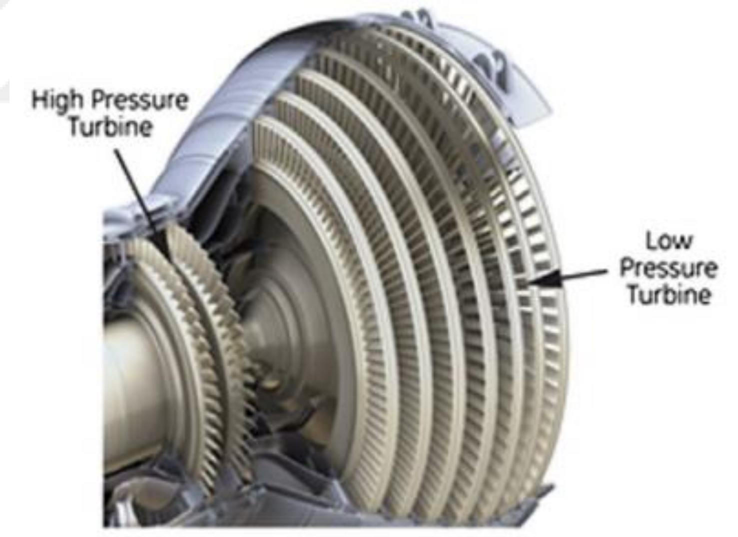

Figure 2-5: Application of TiAl in low pressure turbine section of Boeing GEnx-1B [21].

Many titanium aluminides intermetallic compounds like Ti_3Al (α_2), TiAl (γ), Al_2Ti and Al_3Ti are found stable at room temperature and have studied in the literature, However, the γ-TiAl have been more extensively studied due to its high temperature strength with low density. It took more than 20 years of intensive research to achieve the desired properties of this material and make it commercially available [22].

Property	Ti-Base	Ti_3Al (α_2)-Base	TiAl (γ)-Base	Superalloys
Structure	Hcp/bcc	$D0_{19}$	$L1_0$	FCC/$L1_2$
Density (g/cm3)	4.5	4.1-4.7	3.7-3.9	7.9-8.5
Modulus (GPa)	95-115	110-145	160-180	206
Yield strength (MPa)	380-1,150	700-990	350-600	800-1,200
Tensile Strength (MPa)	480-1,200	800-1,140	44-700	1,250-1,450
Room Temperature Ductility (%)	10-25	2-10	1-4	3-25
High Temperature Ductility (%/°C)	12-50	10-20/660	10-600/870	20-80/870
Room-Temp Fracture Toughness (MPa$\sqrt{m}$)	12-50	13-30	12-35	30-100
Creep Limit (°C)	600	750	750*-950[ŧ]	800-1,090
Oxidation (°C)	600	650	800[ŧ]-950[§]	870[ŧ]-1,090[§]

*Duplex microstructures. [ŧ] Fully-lamellar microstructure. [ŧ] Uncoated. [§] Coated/Actively cooled.

Figure 2-6: Properties of Titanium Alloys, titanium Aluminides and Superalloys [23]

In Chapter 4 of this research work, the machining of 48-2-2 γ-TiAl (Ti-48AI-2Nb-2Cr) is performed. 48-2-2 γ-TiAl belongs to 2nd generation γ-TiAl which has fully lamellar structure. It is one of the most successful alloys in this generation with good fracture toughness and ductility. The addition of chromium (Cr) increase the ductility and thereby increase the workability of the material whereas the addition of niobium (Nb) enhance the oxidation resistance and creep resistance [21].

2.4 Cutting force model

Accurate and fast prediction of cutting forces is important in high-performance cutting in the aerospace industry. In order to machine the part, prior knowledge of cutting forces is important as it influence the machine power, the cutting tool life and can cause deflection of the tool and the workpiece. In this section, the cutting force model developed for orthogonal cutting and oblique cutting is discussed in detail.

2.4.1 Orthogonal cutting force model

Orthogonal cutting is the two-dimensional pain strain deformation metal cutting process. In this process, the cutting edge of the tool is perpendicular to the direction of cutting velocity and the cutting is uniform along the cutting edge. A substantial amount of work has been done in the past to develop the analytical model for orthogonal cutting.

Ernst and Merchant [24] developed the orthogonal cutting model based on the shear plane model. This model assumes that the shear stress on the shear plane is equivalent to the yield shear stress of the material. The merchant circle force diagram is shown in Figure 2-7.

Lee and Shaffer [25] introduce the slip line field model for orthogonal cutting based on the rigid perfectly plastic material. Figure 2-8 shows the constructed slip-line field.

Oxley [26] developed the analytical model based on thick shear deformation zone. The model is illustrated in Figure 2-9.

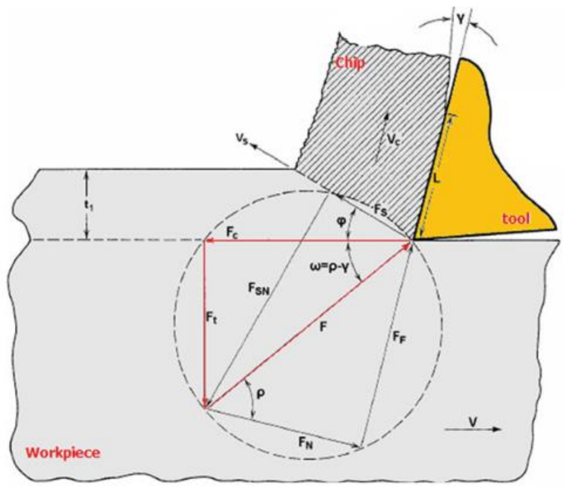

Figure 2-7: Merchant circle diagram [27]

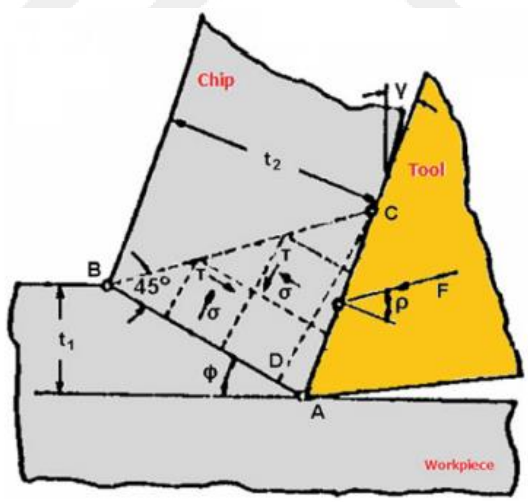

Figure 2-8: Lee and Shaffer's slip-line field model [27]

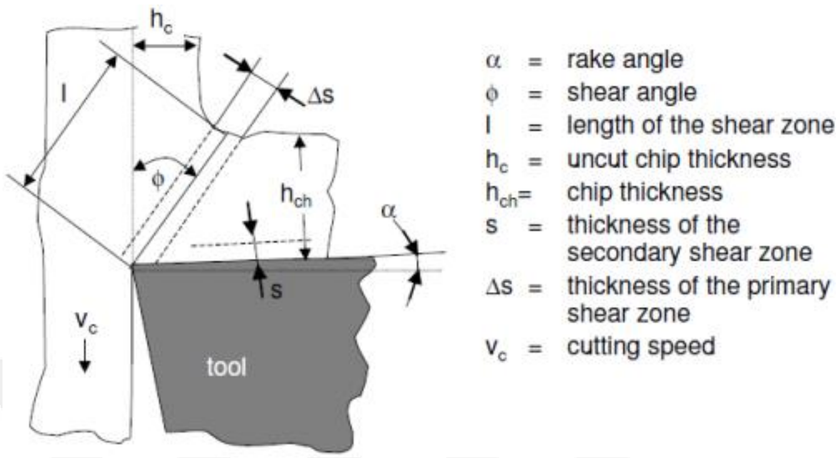

Figure 2-9: Oxley thick shear zone model [28]

All these analytical models have some limitations, as these models cannot predict the type of chip formation and the material behavior in the chip formation area. Owing to these drawbacks, researchers used different numerical methods to simulate the orthogonal cutting process [29–34].

Scherman et al. [33] studied the interaction between the tool and the cutting process by utilizing the computationally intensive Lagrangian technique.

Arrazola and Özel [34] used the Arbitrary Lagrangian-Eulerian (ALE) technique with an explicit solution to simulate the orthogonal cutting process (Figure 2-10). These numerical models provide the advantage to predict the cutting forces, cutting temperature and chip geometry from the machining parameters, however, they are strongly dependent on the modeling assumptions, the modeling approach, the material behavior laws, the friction models and the wear models [35]

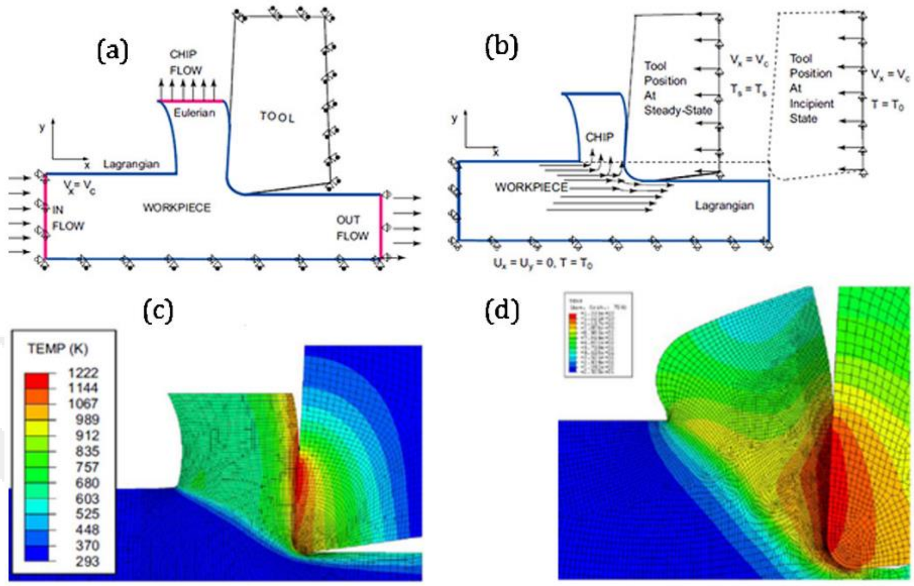

Figure 2-10: FEM models (a) ALE formulation, and (b) pure Lagrangian approach, and the predicted temperature fields, respectively (c) and (d) [34].

2.4.2 Cutting force model for milling process

The prediction of cutting forces in milling operation is more complicated than orthogonal cutting. Variety of helical end mill geometry is used in the industry as shown in Figure 2-11. Flat end mill and ball-end mill are widely used in the machining of aerospace structural parts. Tapered helical end mills are used in five axis machining of jet engine compressors. A significant amount of research has been done to develop the milling cutting force model for different cutter geometries [36–43].

Young et al. [40] utilized the orthogonal machining theory to predict the milling cutting forces depending on the workpiece material properties and cutting conditions.

Engin and Altintas [41] introduced the generalized analytical model for different helical end mills. In this model, the cutting edge point is mathematically expressed along with the helical flute and the cutting forces are predicted by integrating the process along the cutting edge.

Li et al. [42] proposed a model to predict the cutting forces for end milling operation. The model considers the tool geometry, fundamental workpiece material properties, and the cutting conditions. To obtain the cutting force, the end mill is discretized into a number of slices along the cutter (Figure 2-12) and the cutting force on each slice is calculated using oblique cutting models and milling cutter geometry. Then, the calculated cutting force of all cutting slices of all cutter tooth are summed to predict the total cutting force acting on the cutter. Experimental milling tests are performed to validate the approach. A good agreement between the experimental and simulated results was obtained.

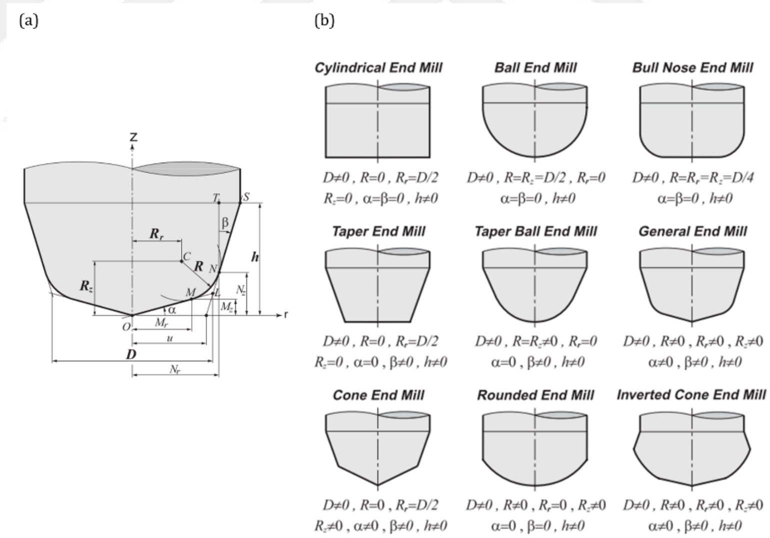

Figure 2-11: Helical milling cutter geometries, (a) General tool geometry, (b) End mill shapes [41]

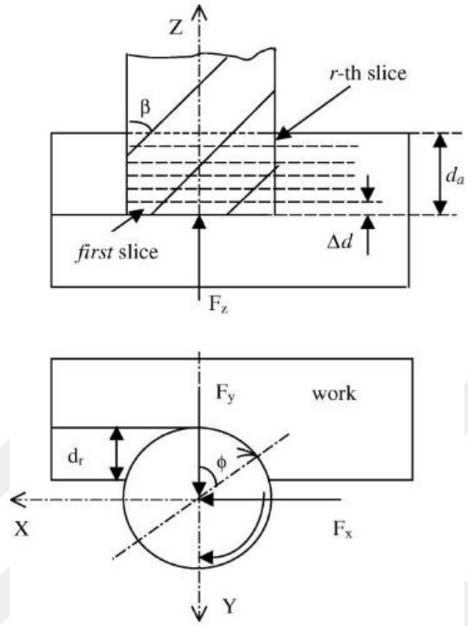

Figure 2-12: Discretization of milling cutter into slices [42].

Lazoglu and Liang [43] established the analytical expression for the prediction of dynamic cutting forces in ball-end milling. In this model, the cutter workpiece interaction is characterized using chip width density function.

Altintas and Lee [44] proposed the analytical model to predict the cutting forces, surface finish, and chatter stability lobes in ball-end milling operation. In this model, true trochoidal motion of ball end cutter is modeled, and the dynamically regenerated chip thickness is evaluated at a discrete time interval.

lazoglu [45] presented the new mechanistic model to predict the cutting force in ball-end milling of sculptured surfaces. In this model, the intersection domain between the workpiece and the tool is calculated and used in the cutting force prediction as illustrated in Figure 2-13.

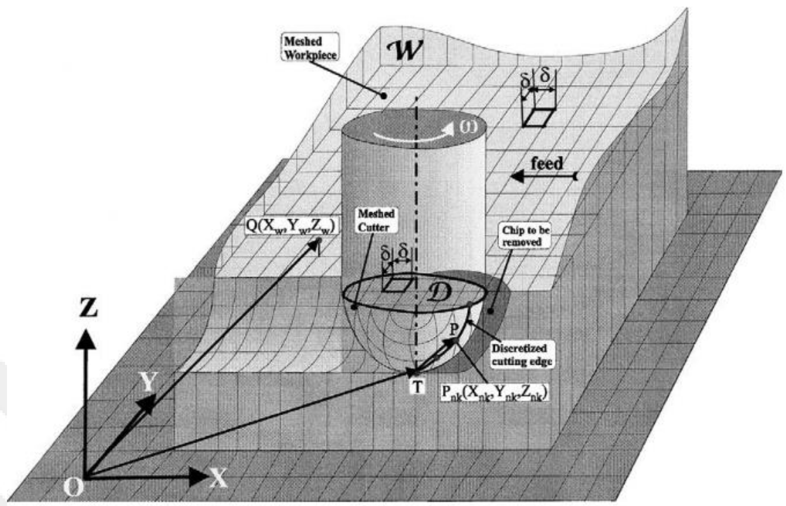

Figure 2-13: Illustration of meshed workpiece and cutter engagement domain [45]

With the advancement of computational technology, several researchers studied the numerical model to predict the cutting forces. Özel and Altan [46] simulated the flat end milling cutting process and predicted the chip flow, cutting forces, tool stress and cutting temperature. The simulation is performed using commercial software DEFORM-2D^{TM}. The chip formation at the primary and secondary cutting edges of the tool is predicted by utilizing the plain strain and axisymmetric workpiece deformation model. Experimental validation of the model is done by performing dry machining experiments for slot milling.

Mehdi and Zghal [47] proposed the numerical model to predict the dynamic cutting forces in peripheral milling. In the study, the effect of tool parameters on process damping and cutting forces are discussed. The advantage of using numerical model is that it can imitate the cutting process more realistically and is able to predict the process parameters such as cutting forces, temperature, chip flow, stresses precisely, however, the practical application of these models for analyzing the cutting forces are limited due to their high computational cost.

2.4.3 Identification of cutting force coefficients for force model

The most common method used for analyzing the cutting forces is the analytical mechanistic cutting force model. In this model, the cutting forces are formulated as a function of cutting coefficients. The accuracy of the analytical model is highly dependent upon the accurate prediction of the cutting force coefficients and edge coefficients. Different approaches have been suggested in the literature to predict the cutting coefficients.

Authors in [44,48] used the orthogonal cutting data to calculate the cutting coefficients. This technique is based on the orthogonal process to oblique process transformation. In this technique, the chip thickness and the cutting forces are measured in the tangential and feed directions in an orthogonal turning test. The measurements are used to calculate the fundamental cutting parameters, including shear stress, shear angle and friction angle. Transformation of these parameters is then utilized to model oblique cutting processes such as the milling operation. The advantage of using orthogonal to oblique transformation technique over other methods is that the cutting coefficients can be predicted before the manufacturing of the tool. This method is independent of cutter geometry and can be used to simulate the cutting forces for any metal cutting process alike.

Gradišek et al.[49] presented the general approach to identify the cutting coefficients for a general helical end mill. In mechanistic calibration, several cutting tests are required with different feed rates in order to generate the coefficients for different work/tool material combinations, tool coatings, and geometries. This calibration method provides the accurate prediction of cutting coefficients, However, the method is tool and workpiece dependent. If the geometry or material of tool-workpiece pairs changes, the calibration tests need to be conducted again.

Yao et al. [50] proposed the chatter free, cylindrical surface milling method to calculate the cutting coefficients for ball-end milling. In this approach, the effect of tool inclination and tool runout is considered.

Layegh and Lazoglu [51] introduced the new strategy for the identification of cutting coefficient for ball-end milling of free form surfaces for each cutting disk. The ball part of the tool is divided into the number of disks and the experimental setup is designed to cut the workpiece while only that disk is in contact with the workpiece as shown in Figure 2-14. The validation of this strategy is demonstrated experimentally.

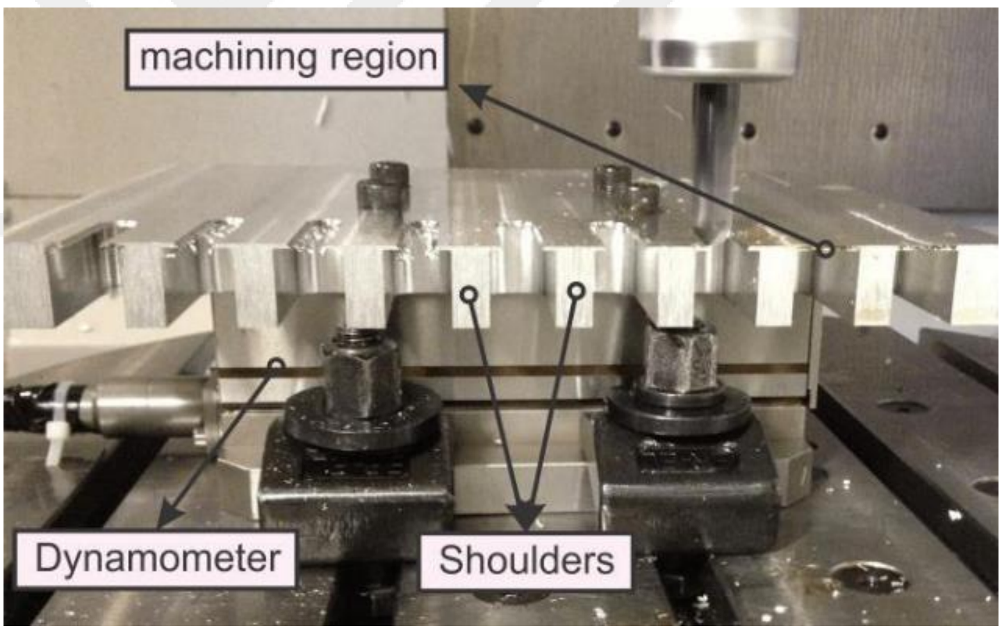

Figure 2-14: Experimental setup for cutting coefficient identification [51].

2.5 Heat load during machining

During machining, the heat is generated due to the plastic deformation in the shearing zone and the friction between the tool and the workpiece [52]. Around 80% of the generated heat carried out by the chips while the remaining heat is dissipated into the tool and the workpiece [53], therefore increases the temperature of the tool, workpiece, and chip. In machining, the temperature is one of the critical factors affecting the part quality, thermal and residual stresses, part distortions and tool wear. Owing to these reasons, the modeling of heat load during machining is important.

A vast number of contributions has been made to predict and measure the cutting temperature of tool, workpiece, and chips during machining. Several techniques have been used to determine the cutting temperature, including experimental, analytical, finite difference method (FDM) and finite element modeling (FEM) [35].

Kim et al. [54] used the implanted thermocouple technique to measure the cutting temperature in the high speed ball-end milling. Dry, wet and compressed chilled air cutting environment were investigated and the shear zone cutting temperature was measured.

Ming et al. [55] developed the model to calculate the heat flux and the temperature distribution on the tool-workpiece interface. The model was based on inverse heat transfer conduction theory and applied to study the temperature distribution in thin-walled machined part on high speed machining. The model was validated by measuring the surface temperature of the thin-walled part using the infrared thermometer and the tool-workpiece interface by an artificial thermocouple.

Lazoglu et al. [56] used the analytical hybrid approach to predict the temperature in drilling Ti-6Al-4V with carbide tools. The novel thermocouple based experimental setup is introduced in the study to measure the temperature evolution in drilling (Figure 2-15). A device named Rotary Tool Temperature (RTT) is designed to measure the temperature of the drilling tool close to the cutting edge.

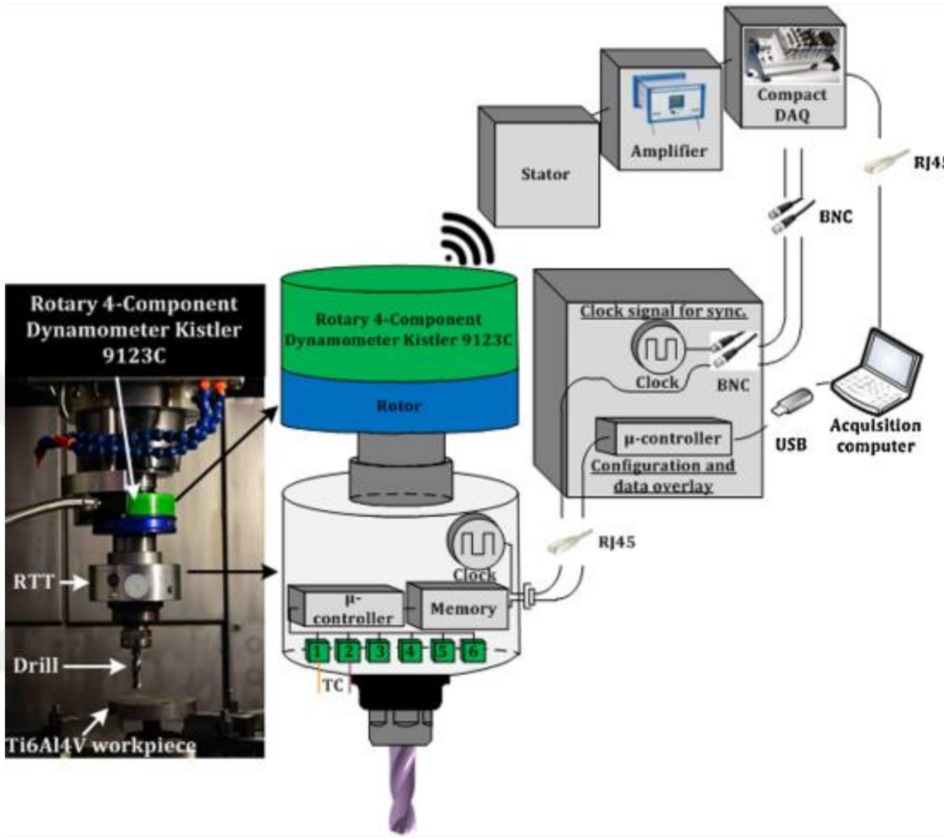

Figure 2-15: Experimental setup to acquire the temperature during drilling [56]

Komanduri and Hou [57] developed the analytical model to predict the temperature distribution in metal cutting. In the study, Hahn's moving oblique band heat source solution and modified Jaeger's moving band heat source solution is used for the shear plane heat source and the tool-chip interface frictional heat source (Figure 2-16). The model is applied for the machining of steel with carbide tools and good agreement found between the simulation and the analytical model.

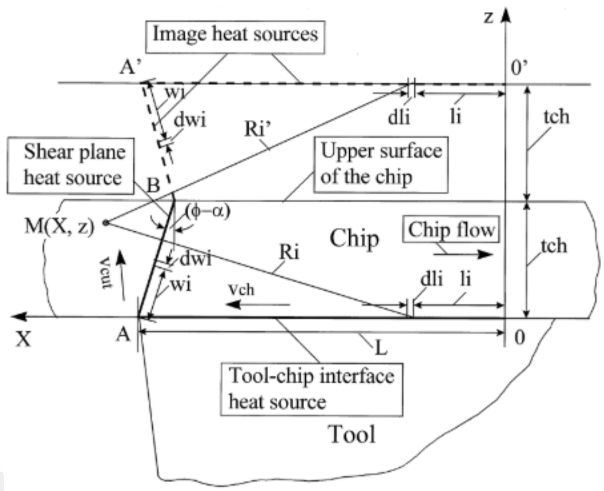

Figure 2-16: Schematic of heat transfer model with the shear plane and frictional plane heat source [57]

Lazoglu and Altintas [58] developed the FDM based numerical model to predict the tool and chip temperature distribution in continuous and interrupted machining operation. The shear energy in the primary zone, the friction energy at the rake face contact and the heat balance between the tool and chip are considered in the model. The temperature field is represented as a first-order dynamic system and the time constant is identified based on thermal properties of tool and workpiece.

Rai and Xirouchakis [59] applied the average shear plane temperature (Oxley’s cutting temperature model) in their finite element model to predict the transient temperature distribution of the workpiece during the material removal process. The authors performed the transient thermal analysis considering the dry and wet machining operations.

Ulutan et al. [60] proposed the FDM based model to predict the three dimensional temperature fields. In the model, the heat balance equations are solved analytically for the tool, chip and the workpiece including the heat convection effect. The model is validated with the infrared thermal measurement from machining of AISI 1050 and AISI H13 material as shown in Figure 2-17.

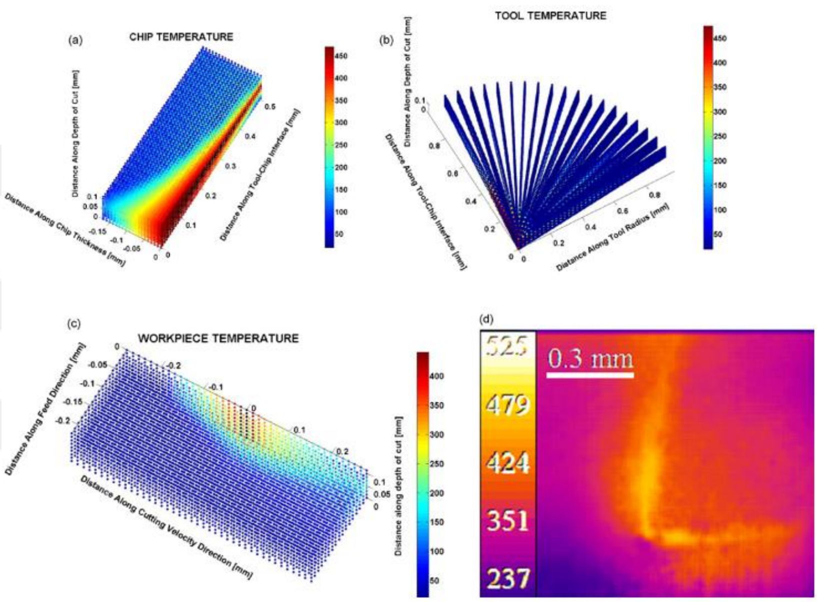

Figure 2-17: Measured and simulated results of temperature for AISI 1050 workpiece and tool having 6° of rake angle, V= 80 m/min and h = 0.1 mm. (a) Simulated chip temperature field. (b) Simulated tool temperature field. (c) Simulated workpiece temperature field. (d) Measured tool temperature field [60]

Lazoglu and Bugdayci [61] introduced the new semi-analytical method for milling processes for determining the temperature fields of the tool. The heat generated by the side cutting edge and bottom cutting edge of the tool is considered in the model. The authors also used various carbide composition tool to study the effect of temperature on tool wear in the machining of aerospace grade Al7050.

Mamedov and lazoglu [62] presented the hybrid model to predict the temperature field of tool and workpiece in micro milling of Ti-6Al-4V. The heat load due to shearing and friction phenomenon are calculated using analytical thermo-mechanical model and applied as an input in the finite element model. The experimental validation of the model is performed by measuring the temperature using a specially design setup with thermocouple (Figure 2-18). The simulated and measured temperature distribution for one of the cases is shown in Figure 2-19.

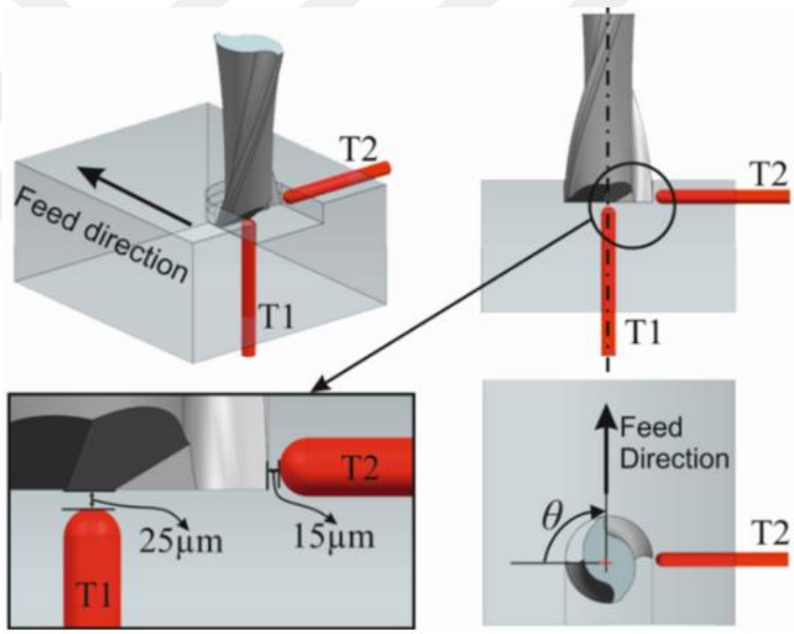

Figure 2-18: Representation of temperature measurement setup [62]

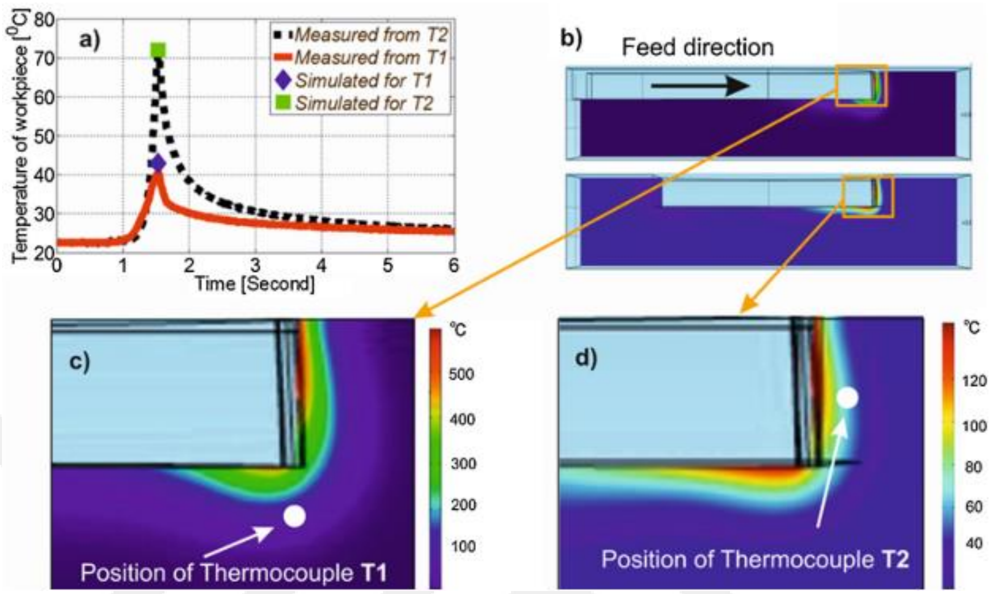

Figure 2-19: (a) Measured and simulated temperature for case 3; (b) Simulated temperature for case 3; (c) Simulated temperature filed at θ = 90°; (d) Simulated temperature field at θ = 180° [62]

2.6 Distortion in thin-wall parts due to machining

Complex thin-wall structural parts are widely used in various industries. Especially in the aerospace industries, these parts are machined with extensive care. The part quality i.e. dimensional and geometrical accuracies are extremely important in the machining of these thin-wall structural parts. These parts are commonly manufactured using the milling process in which up to 90 % of the material is removed. Due to the milling process and low stiffness, the thin-wall structural parts get easily distorted and require time consuming post machining correction. Depending on the dimensional scale and the machining parameters of the thin-wall structural parts, the distortion can range from a few micrometers to several millimeters.

Therefore, due to the milling induced distortion, the production cost becomes unavoidable and, in some cases, excessive distortions may lead to rejection of the expensive aerospace parts. Shearing and friction phenomena during the milling process cause the mechanical and thermal loads, and therefore these loads affect the distortion of the thin-wall structural parts.

The significant amount of research work has been dedicated to distortion prediction of structural parts and residual stresses. In the following section, the previously done research work have been discussed in detail.

Koike et al. [63] designed the method to minimize the static deformation of the workpiece due to cutting forces. They design the algorithm to remove the workpiece elements according to the feed direction and tool orientation (Figure 2-20). The method was experimentally verified by machining titanium cantilever.

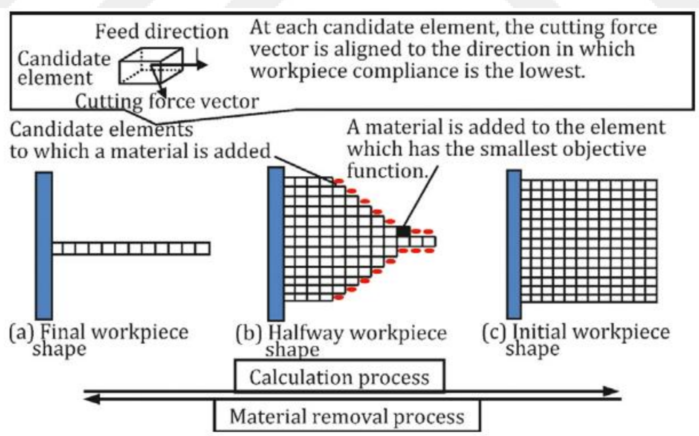

Figure 2-20: Representation of the material removal process [63]

Denkena et al. [64] experimentally studied the effect of machining parameters, cutting edge geometry and tool wear on subsurface residual stresses in the machining of forged aluminum alloy. They found that at higher depth of cut, the increase in feed per tooth, a decrease of the width of cut and higher edge radii leads to the compressive residual stresses.

Brinksmeier and Sölter [65] proposed the method to predict the shape deviation of the complex machined workpiece due to plastic deformation. The model is based on a finite element method and uses the experimentally known stresses as an input. Figure 2-21 illustrates the methodology of the approach.

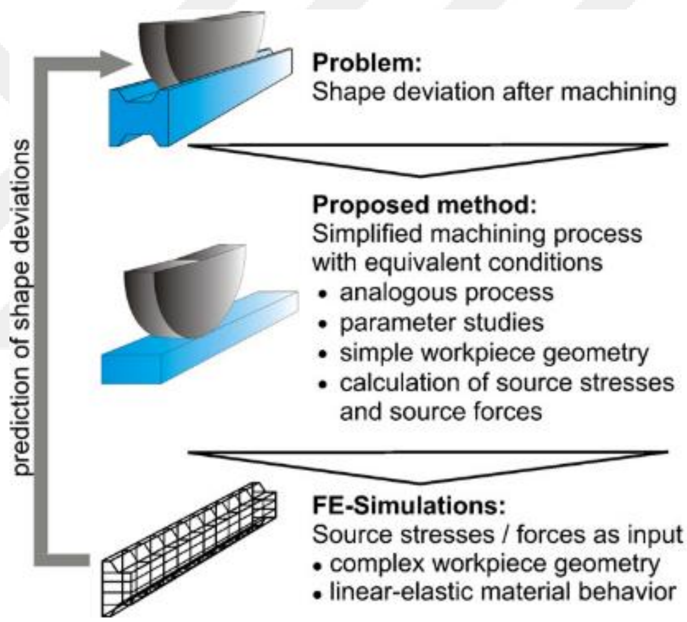

Figure 2-21: Methodology to predict shape deviation [65]

Lazoglu et al. [66] developed an enhanced analytical model to predict the machining induced residual stresses in orthogonal cutting. In the model, the effect of thermal and mechanical stresses is considered, and the relaxation method is used for the plasticity. The model is verified experimentally with X-ray diffraction measurements on waspaloy material. The measured and experimental results for residual stresses are shown in Figure 2-22.

Smith et al. [67] introduced the use of sacrificial structure preforms to minimize the effect of machining on thin-wall finished parts.

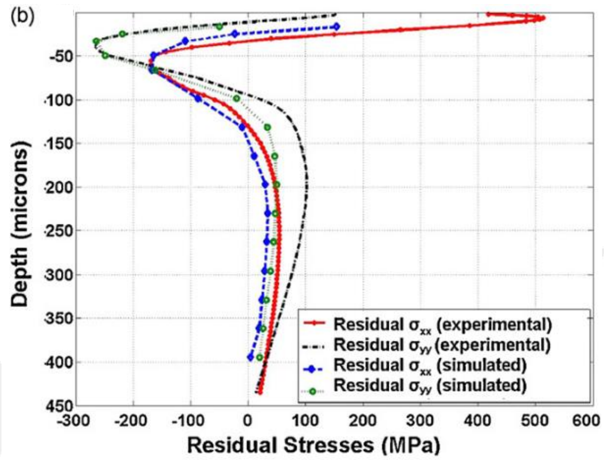

Figure 2-22: Comparison of measured and simulated residual stress profile for V=25 m/min, feedrate 0.075 mm/rev, tool contact radius 51.6 µm and tool rake angle 5° [66]

One of the common methods used to predict the distortion of complex thin-wall structural parts considering the thermo-mechanical load is the finite element method (FEM). The advantage of using this method is that it can imitate the cutting process more realistically and handle the complex parts. However, the simulation method adopted by researchers are different.

Ratchev et al. [68] proposed a simulation environment to predict the mechanical workpiece deflection. They incorporated the effect of cutting forces and material removal in the model. However, the influence of thermal effects on deflection was not considered. The system integration in the simulation environment is shown in Figure 2-23.

Rai and Xirouchakis [69] developed the FEM based process plan verification system to predict the elastic plastic deformation of the thin-wall prismatic parts during the milling operation. The simulations are performed on aerospace grade aluminum 7050. In this model, the effect of thermo-mechanical load, fixturing, cutting sequence, toolpath and cutting parameters are considered. However, the presented system is computationally expensive which makes it limitation for particle use. The system modular architecture is shown in Figure 2-24.

Denkena et al. [70] experimentally studied the shape deviation in the machining of thin-wall structural parts. The authors also used FEM model to separately investigate the influence of thermal deviation and force induced deviation.

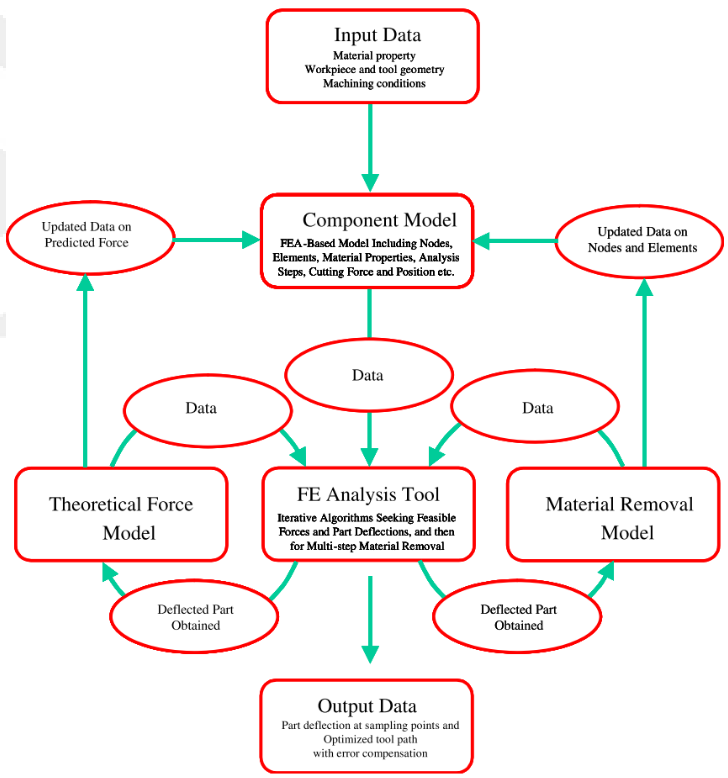

Figure 2-23: Architecture of the simulation environment [68]

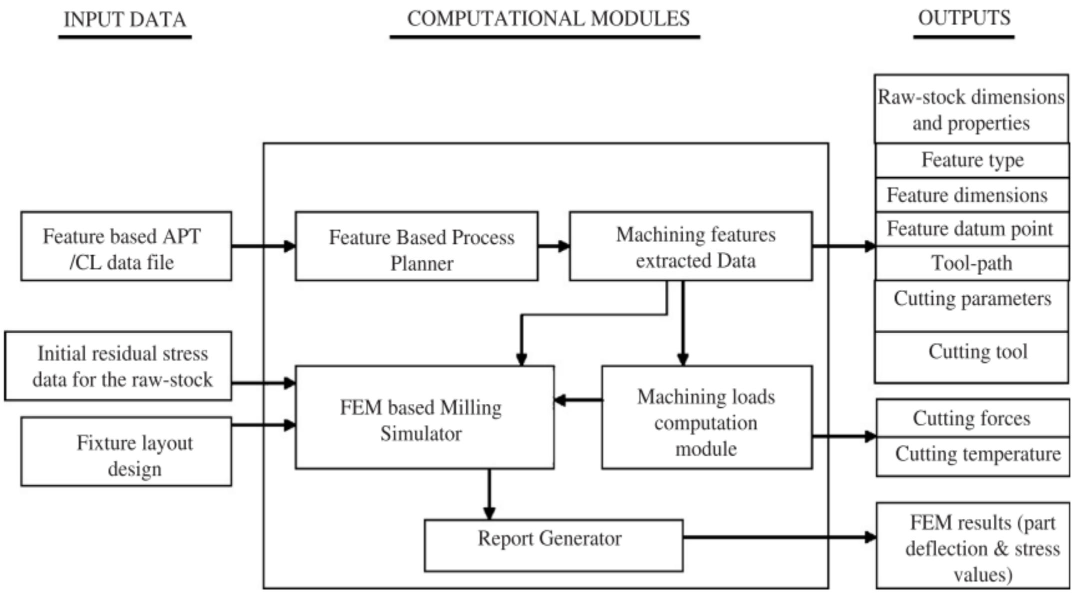

Figure 2-24: Simulation environment architect module [69]

Lazoglu and Mamedov [71] introduced the new modeling approach to predict the deformation of thin-wall parts in micro machining. In the modeling approach, the elastic-plastic deformation is predicted considering the thermo-mechanical load in micro milling. The cutting and heat load are estimated using an analytical model and used as an input for the FEM model. The developed model is validated under various cutting conditions in micro milling of Ti-6Al-4V and the deformation is measured using online laser displacement sensor and offline white light interferometer (WLI), as shown in Figure 2-25. However, the developed model is two dimensional and needs to extend to three dimensions for practical implementation.

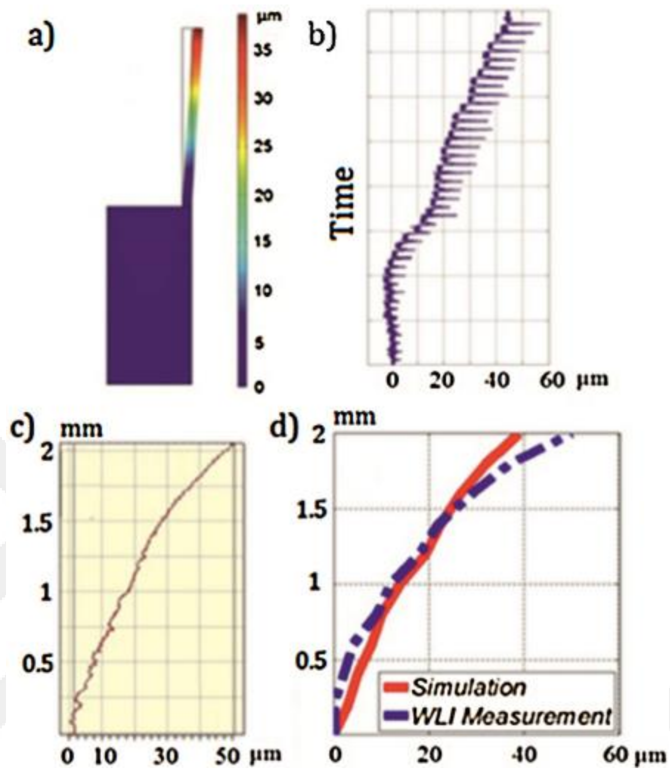

Figure 2-25: Simulated and experimentally measured deformation for V= 25 m/min, axial depth = 50 µm and feedrate = 200 mm/min, (a) FEM result, (b) measured online deformation with laser sensor, (c) deformation measured with WLI, (d) comparison between simulated and measured deformation [71]

Despite the aforementioned efforts, there is a need to develop the distortion prediction model for complex thin-wall structural parts. Therefore, Chapter 3 of this thesis presents the model for the distortion prediction of complex thin-wall parts by combining the effect of mechanical and thermal loads. The validation of the model is performed through milling experiments and with online and offline deformation measurements.

2.7 Machining of Gamma titanium aluminide

γ-TiAl is one of the important materials in the aerospace industry due to its superior thermo-mechanical properties [72,73]. As it has been shown in several conventional machining publications, machinability of γ-TiAl is poor because of its low ductility combined with high hardness and brittleness at room temperature, low thermal expansion, low fracture toughness and chemical reactivity with many tool materials [74,75]. In consequence, the machining cost is high, which can restrict the widespread use of these materials in the industry. Several research studies have been carried out in the last years dealing with the machinability properties of γ-TiAl.

Mantle et al. [76]investigated the surface integrity of γ-TiAl, Ti-45Al-2Nb-2Mn-0.8 vol.% TiB2XD by performing high speed milling operations. Experiments were carried out using coated tungsten carbide ball-end mill in up milling and down milling directions.

Priarone et al. [77] studied the effect of cutting tool angles and cutting-edge preparation in machinability of Ti-48Al-2Cr-2Nb EBM sintered γ-TiAl. All the milling operations were performed in down milling mode with coated and uncoated carbide end mills.

Beranoagirre et al. [78] provided the specific cutting force coefficients obtained from mechanistic calibration method for three different types of γ-TiAl alloys: the MoCuSi type in ingot and extruded form, and the TNB type in ingot form. They performed milling experiments and studied the tool wear for different cutting conditions and found that the cutting speed is the determining factor in tool life.

Settineri et al. [79] performed turning and milling experiments on three different γ-TiAl alloys: Ti–48Al–2Cr– 2Nb, Ti–43.5Al–4Nb–1Mo–0.1B, and Ti–45Al–2Nb–2Mn - 0.8 vol.% TiB2 XD, focusing on machinability and material characterization. The experimental results were extremely dissimilar due to the different alloying elements which affected the mechanical and thermal material properties.

Hood et al. [80] investigated the surface integrity by performing slot milling on Ti-45Al-2Nb-2Mn-0.8 vol.%, TiB2 using AlTiN coated WC ball nose end mills.

The research work in Chapter 4 presents the creation of orthogonal database for 48-2-2 γ-TiAl which is first time reported in the literature. The database is then used for the prediction of accurate cutting forces employed in high-performance machining of aeronautic components such as blades.

Chapter 3
DISTORTION MODELING OF THIN-WALL STRUCTURAL PARTS

3.1 Overview

The demand for the new planes in the aerospace industry is increasing due to the significant rise in air traffic. This represents the increase in the manufacturing of high-quality parts. The accuracy of the parts is highly dependent on the manufacturing process. The cutting and thermal load during machining process directly affects the thin-wall part distortion and leads to the part rejection. Currently, there is a lack of approach to predict the geometrical and dimensional instabilities in complex thin-wall structural parts considering the combined effect of cutting and thermal load. Therefore, there is a need to model the thin-wall part distortion due to the effect of cutting and thermal load.

In this chapter, a model is developed to investigate the machining induced distortion of complex thin-wall structural parts made of Al7050 T7451 using finite element model. Key factors influencing distortion such as mechanical and thermal loads are considered in the model and estimated analytically. These loads are used as an input in the model and are applied to the final part geometry using the proposed approach. The model is validated for complex geometry. Real-time cutting forces, temperature, and laser displacement measurements and offline measurement with coordinate measurement machine (CMM) are acquired and compared with the numerical results.

3.2 Modeling thermo-mechanical load

During the milling process, the joint action of cutting forces and cutting heat lead to notable distortion. Especially, in the thin-wall structural parts when the thickness of the material is below 3 mm, the machining-induced thermo-mechanical loads play a leading role in the part distortion [81]. Substantially, these loads are highly influenced by the cutting parameters used for the machining of structural parts. The variation in cutting parameters and tool geometries produce the strong thermal-force coupling field that causes the plastic deformation and leads to part distortion. Therefore, to predict the distortion of thin-wall structural part the precise estimation of mechanical and thermal loads is required.

3.2.1 Modeling of cutting forces

The accurate and fast prediction of cutting force is important for the machining process. The knowledge of cutting force prior to the machining operation helps in tool design and process parameter optimization to avoid chatter, tool wear, and get the good surface quality of the part.

In the present study, the analytical mechanistic cutting force model is implemented to calculate the cutting forces required in the distortion prediction model. The mechanistic cutting force model provides the fast and accurate prediction of cutting forces in which the cutting force is a linear function of uncut chip thickness area and cutting coefficients.

In the model, the helical end mill cutter is discretized into a number of disks along its axis and the differential cutting forces are calculated as follows:

$$
\begin{aligned}
dF_{t,j}(\theta,z) &= \left[K_{tc}h_j\left(\theta_j(z)\right)+K_{te}\right]dz\\
dF_{r,j}(\theta,z) &= \left[K_{rc}h_j\left(\theta_j(z)\right)+K_{re}\right]dz\\
dF_{a,j}(\theta,z) &= \left[K_{ac}h_j\left(\theta_j(z)\right)+K_{ae}\right]dz
\end{aligned}
$$

Equation 3-1

Here, dF_t, dF_r and dF_a are the differential tangential, radial and axial forces. Moreover, θ represents the tool immersion angle, j, $z, h,$ and d_z are respectively the flute number, axial depth of cut, uncut chip thickness and elemental length of the cutting edge in the axial direction. K_{tc} , K_{rc}, and K_{ac} are the specific cutting coefficients, K_{te}, K_{re} and K_{ae} are the edge coefficients. These coefficients are related to the cutting and ploughing phenomena in metal cutting and are modeled according to the procedure given in [82].

The differential cutting forces in feed (x), crossfeed (y) and axial (z) direction are calculated using transformation matrix as follows:

$$dF_{x,j}(\theta_j(z)) = -dF_{t,j}\cos\theta_j(z) - dF_{r,j}\sin\theta_j(z)$$
$$dF_{y,j}(\theta_j(z)) = dF_{t,j}\sin\theta_j(z) - dF_{r,j}\cos\theta_j(z) \qquad \text{Equation 3-2}$$
$$dF_{z,j}(\theta_j(z)) = dF_{a,j}$$

Here, dF_x, dF_y and dF_z are the differential feed (x), crossfeed (y) and axial (z) forces.

The summation of differential cutting forces of each tooth at every disk is done to obtain the total cutting forces (F_x, F_y, and F_z) in the end milling using Equation 3-3:

$$\begin{bmatrix} F_x \\ F_y \\ F_z \end{bmatrix} = \sum_{j=1}^{N}\sum_{i=z_1}^{z_2} \begin{bmatrix} dF_x \\ dF_y \\ dF_z \end{bmatrix} \qquad \text{Equation 3-3}$$

Here N is the total number of flutes and z_1 and z_2 are the lower and upper limit of axial engagement.

The cutting forces during the milling experiments are measured using table type dynamometer and compared with the simulated forces. Results are shown later in this chapter.

3.2.2 Modeling of heat load

In the present work, the thermal model is developed to predict the temperature field in the workpiece. In order to predict the temperature, the total heat generation rate is analytically calculated. It is assumed that the total heat generation is the sum of heat generation due to shearing and friction in the primary and secondary zones. In order to calculate the heat generation, the previously estimated cutting forces is used.

The heat generation rate in the primary deformation zone and the secondary deformation zone due to shearing and friction is calculated as:

$$\dot{Q}_s(\theta) = F_s(\theta).V_s = \frac{V.\tau_s.a.h(\theta).cos(\alpha_n)}{cos(\emptyset_n - \alpha_n).sin(\emptyset_c)} \quad \text{Equation 3-4}$$

$$\dot{Q}_f(\theta) = F_u(\theta).V_c = \frac{V.F_R(\theta).sin(\emptyset_n).sin(\beta_a)}{cos(\emptyset_n - \alpha_n)} \quad \text{Equation 3-5}$$

Here $\dot{Q}_s$, $\dot{Q}_f$, F_s, F_u, F_R, V_s, V_c, V, τ_s, a, h, α_n, β_a, $\emptyset_n$, $\emptyset_c$ and θ represents the shearing power, friction power, shear force on shear plane, friction force on rake face, resultant cutting force, shear velocity, chip velocity, cutting velocity, average shear flow stress, depth of cut, uncut chip thickness, normal rake angle, friction angle, normal shear angle, shear angle and, the immersion angle.

The total heat generation rate $\dot{Q}_T$ is predicted as follows:

$$\dot{Q}_T(\theta) = \dot{Q}_s(\theta) + \dot{Q}_f(\theta) \quad \text{Equation 3-6}$$

The amount of heat flow into the workpiece $\dot{Q}_W$ is calculated as:

$$\dot{Q}_W(\theta) = \dot{Q}_T(\theta) \times P_W \quad \text{Equation 3-7}$$

Here P_W represents the fraction of total heat flow into the workpiece and depends on the process and workpiece properties (a value of 0.30-0.40 is generally taken for aluminum alloy [59]). In the present work, P_W is set to 0.30.

3.3 Finite element simulation

A finite element simulation for distortion prediction of complex thin-wall part is performed on commercially available ABAQUS solver. The milling process is simulated as a transient coupled field analysis in which the temperature and displacements are simultaneously solved. The simulation environment is developed in Python language to control the whole milling processes includes importing workpiece CAD geometry, generation of mesh, generation of node set, generation of element set, creating time step, applying material mechanical and thermal properties, applying mechanical and thermal boundary conditions, and thermo-mechanical loads. Figure 3-1 illustrates the FEM model architecture and the simulation procedure.

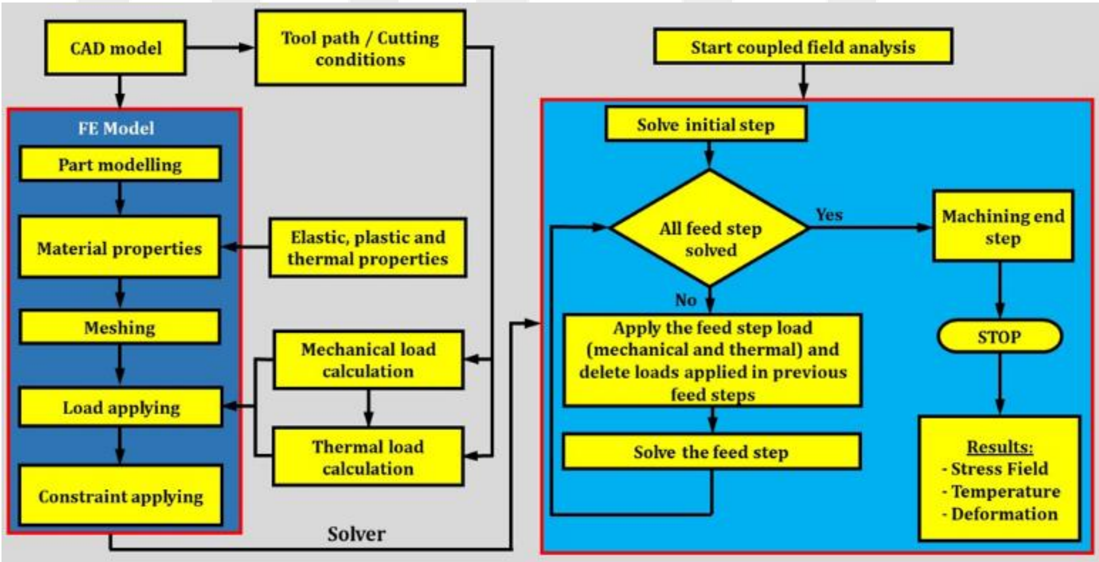

Figure 3-1: Architecture of the FEM model.

To visualize the plastic deformation, the elastic-plastic constitutive model is used in which the linear elasticity and von Mises plasticity with isotropic hardening is employed. In the elastic-plastic constitutive model the total strain is calculated as the summation of elastic and plastic strains as represented in Equation 3-8:

$$d\varepsilon_{total} = d\varepsilon_{elastic} + d\varepsilon_{plastic} \quad \text{Equation 3-8}$$

Here $d\varepsilon_{elastic}$ is the elastic strain which is fully recoverable and $d\varepsilon_{plastic}$ is the plastic strain which cannot be recovered. The plasticity in the model is introduced by using the true stress versus true plastic strain curve for the Al7050 T7451 material as shown in Figure 3-2.

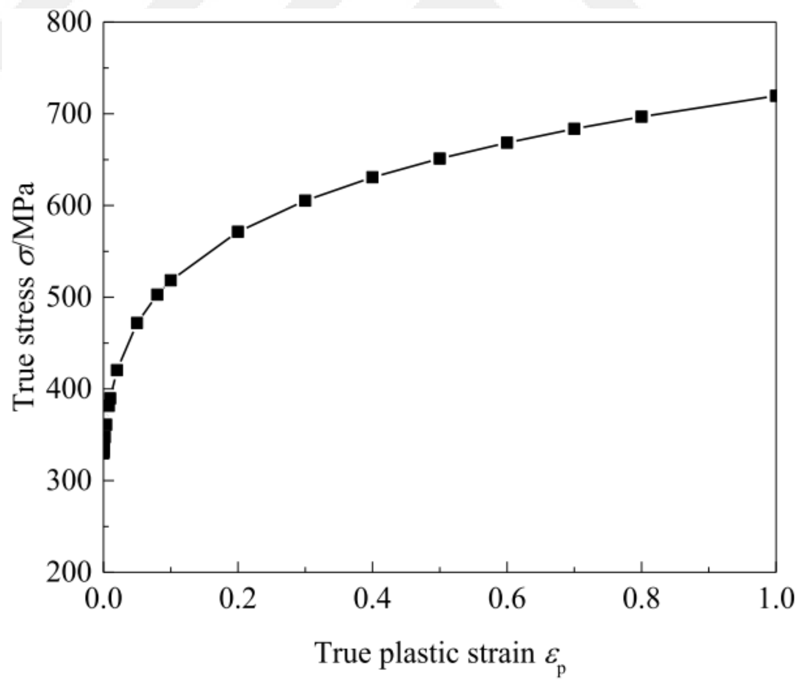

Figure 3-2: Aluminum alloy 7050-T7451 hardening curve [83]

Aerospace grade Aluminum 7050-T7451 has the best combination of strength, stress corrosion and cracking (SCC) resistance, and toughness. Owing to these properties, Al7050 T7451 is one of the important materials used in the aerospace industry for the machining of structural thin-wall parts. The mechanical properties of the material are shown in Table 3-1.

Table 3-1: Mechanical properties of Aluminum 7050-T7451.

Density (ρ)	2830 Kg/m3
Modulus of elasticity (*E*)	71.7 GPa
Poisson's ratio (ν)	0.33
Thermal conductivity (λ)	157 W/m°C
Specific heat capacity (S)	0.86 J/g°C
Coefficient of thermal expansion (α)	25.4×10-6

3.3.1 Strategy for load application

To apply the load on the final workpiece geometry a method is adopted for the application of thermo-mechanical load to the corresponding nodes of the feed-step element as shown in Figure 3-3. Firstly, the mechanical and thermal loads are calculated from the analytical model presented in section 3.2. Then the loads acting on the cutter exit angle (Equation 3-9) is obtained and discretized along the axial segment (depth of cut) of the feed-step element. Finally, the obtained discrete loads in the (feed, crossfeed and axial) direction are applied to the relevant nodes. The similar strategy is used to apply the heat load on the corresponding nodes. To automate the process of node selection and to apply the load along the tool path, a class is constructed in object-oriented programming language Python. The flowchart for the node selection is shown in Figure 3-4. An illustration of cutting load (cutting forces) applied to the model according to the feed direction and the tool rotation is shown in Figure 3-5.

$$\theta_{exit} = \cos^{-1}\left(\frac{R - a_e}{R}\right) \qquad \text{Equation 3-9}$$

Here θ_{exit} is the cutter exit angle, R is the tool radius and a_e represents the width of cut.

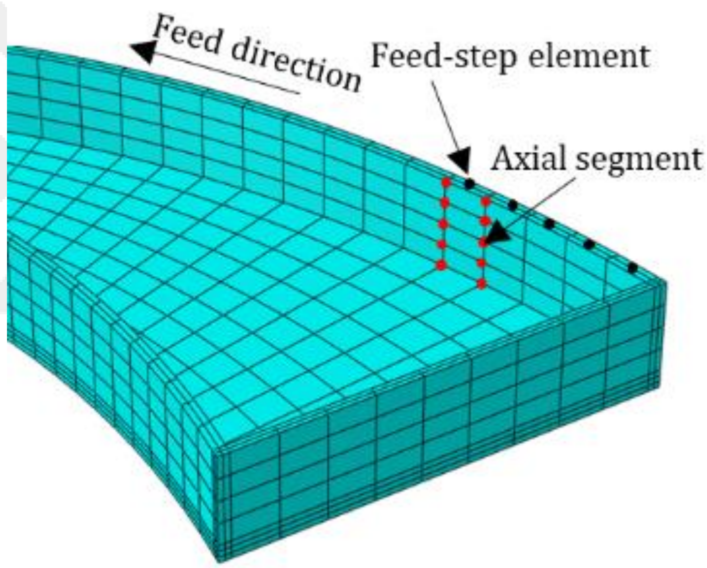

Figure 3-3: Load application strategy.

The time-step for each feed-step is obtained by dividing the machining time corresponding to the tool pass by the number of feed-step elements. Since the load is applied to the wall, the duration of its application is important. For this purpose, the tabular method is used in which the load amplitude is divided between one cutter rotation time period and the remaining time step.

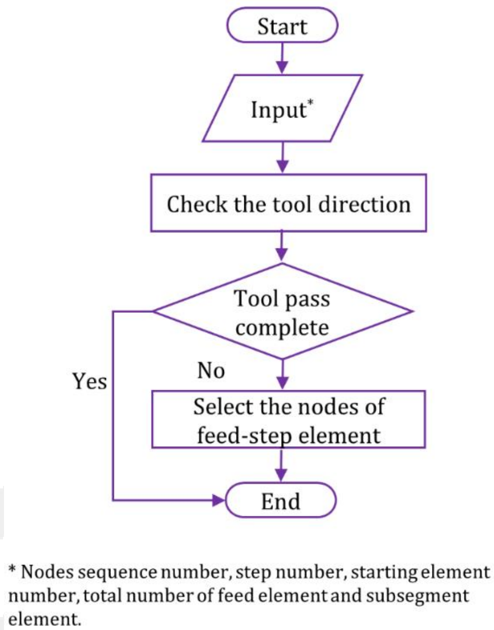

Figure 3-4: Flowchart for node selection.

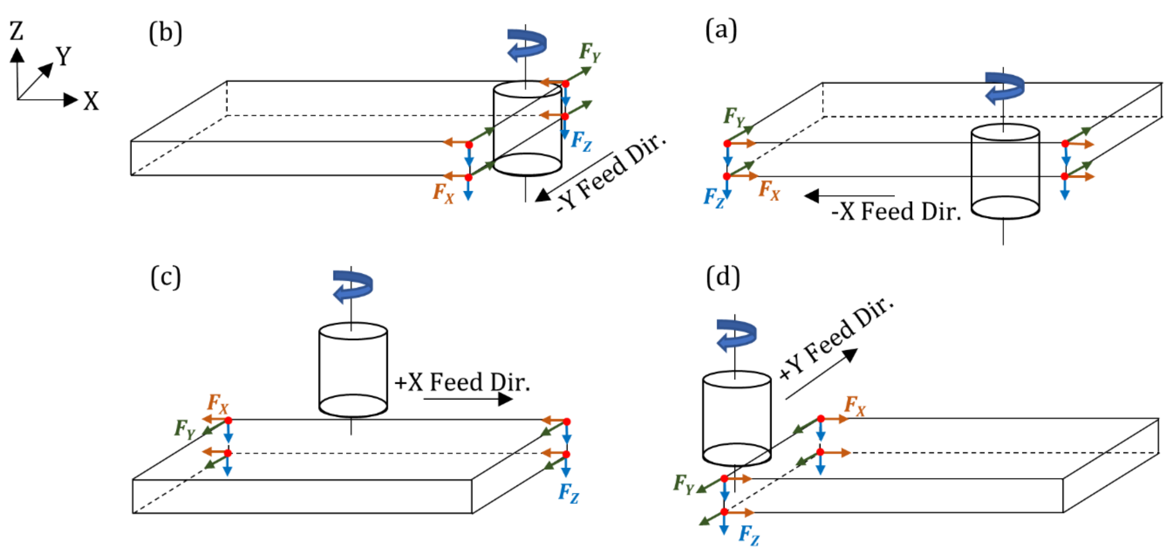

Figure 3-5: Applied cutting forces in the, (a) -X direction, (b) -Y direction, (c) +X direction, (d) +Y direction.

3.3.2 Simulation model

The parts used in the aerospace industries are consists of thin-walls and pockets. Therefore, to predict the distortion, the proposed method is applied on a complex curved shaped thin-wall part having two pockets. The part dimensions are shown in Figure 3-6(a). The thickness of the wall and the rib is 1.4 mm.

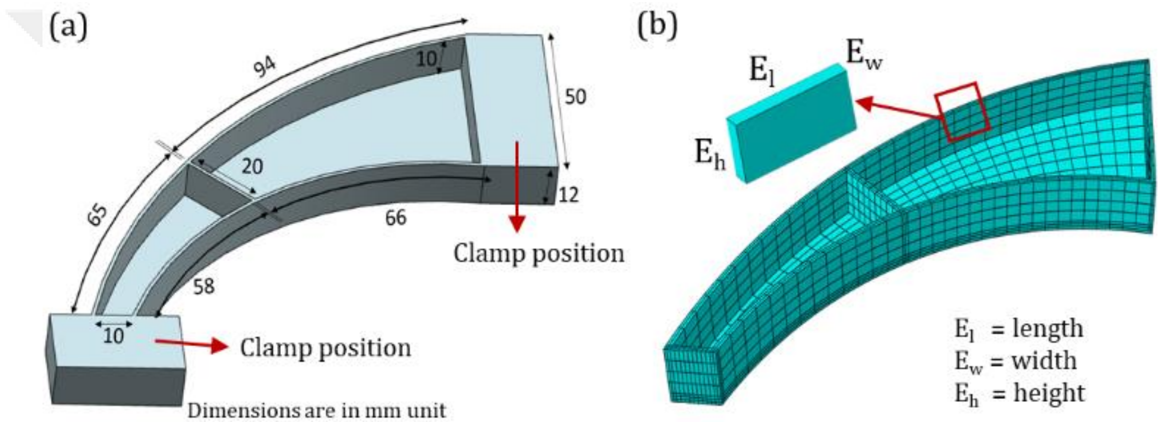

Figure 3-6: (a) CAD model of the workpiece, (b) Meshing of the FE model.

The model is meshed with C3D8T hexahedral elements, an 8-node trilinear element used for coupled displacement and temperature analysis. The total number of elements and nodes in the model is 2306 and 3408 (Figure 3-6(b)). The height and width of the elements on the rib and the wall are set to 2.5 mm and 1.4 mm. Due to the curved geometry, the minimum and maximum length of elements are 2.5 mm and 5 mm.

Clamps are very important elements of machining setup and are used to immobilize the part during the machining. The contact surfaces of the clamps exert the force on the workpiece and can lead to the workpiece deformation. Therefore, the proper selection of clamping position is necessary to avoid the effect of clamping on distortion. In the study, the mechanical boundary constraint is applied to the bottom surface, and the workpiece clamped location as shown in Figure 3-6(a). To apply the thermal boundary condition, convective air cooling with a heat transfer coefficient of 450 W/m^2K for compressed air cooling [84] is applied to the outer wall surfaces. The machining strategy and the tool path is shown in Figure 3-7. The tool passes from the first to the second pocket. The outer tool path will have maximum effect on the thin-wall distortion, therefore, only the outer tool path is considered in the model and the load is applied on the wall. The coupled thermal displacement analysis is performed on a Xeon(R) CPU 3.00 GHz with 64 GB RAM. The complete analysis took approximately 300 minutes of computational time.

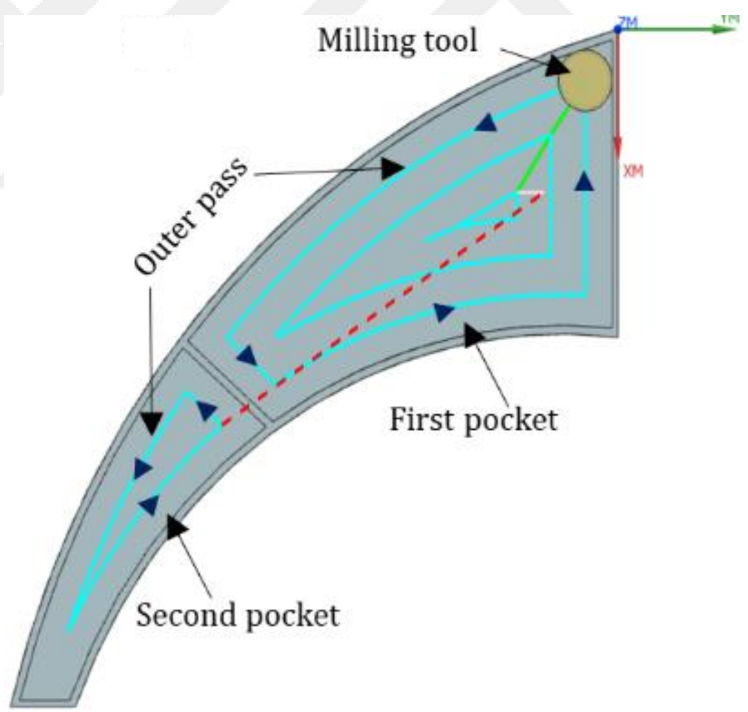

Figure 3-7: Workpiece tool path.

3.4 Experimental setup and validation

Experiments are performed on a 5-axis Mori Seiki NMV5000DCG machining center. Cutting conditions used for the experiments are tabulated in Table 3-2. Cutting forces are measured with a Kistler 9257B table type dynamometer and a high speed data acquisition system. Six J-type thermocouples are used to measure the temperature on the walls. The MX-2 thermal compound with high thermal conductivity is used to minimize the temperature losses. The online deformation of the workpiece during the machining operation is measured by using two Keyence LK-H052 laser sensors. The designed experimental setup and the location of the sensors are shown in Figure 3-8.

Table 3-2: Cutting conditions.

Tool diameter	10 mm
Rake angle	13.6°
Helix angle	25°
Number of flutes	2
Cutting speed	94 m/min
Spindle speed	3000 rpm
Feedrate	480 mm/min
Axial depth of cut	10 mm
Radial depth of cut	7 mm
Shear stress of Al7050 T7451	303.5 MPa
Shear angle	31 °
Friction angle	32 °
Kte	33 N/mm
Kre	20 N/mm

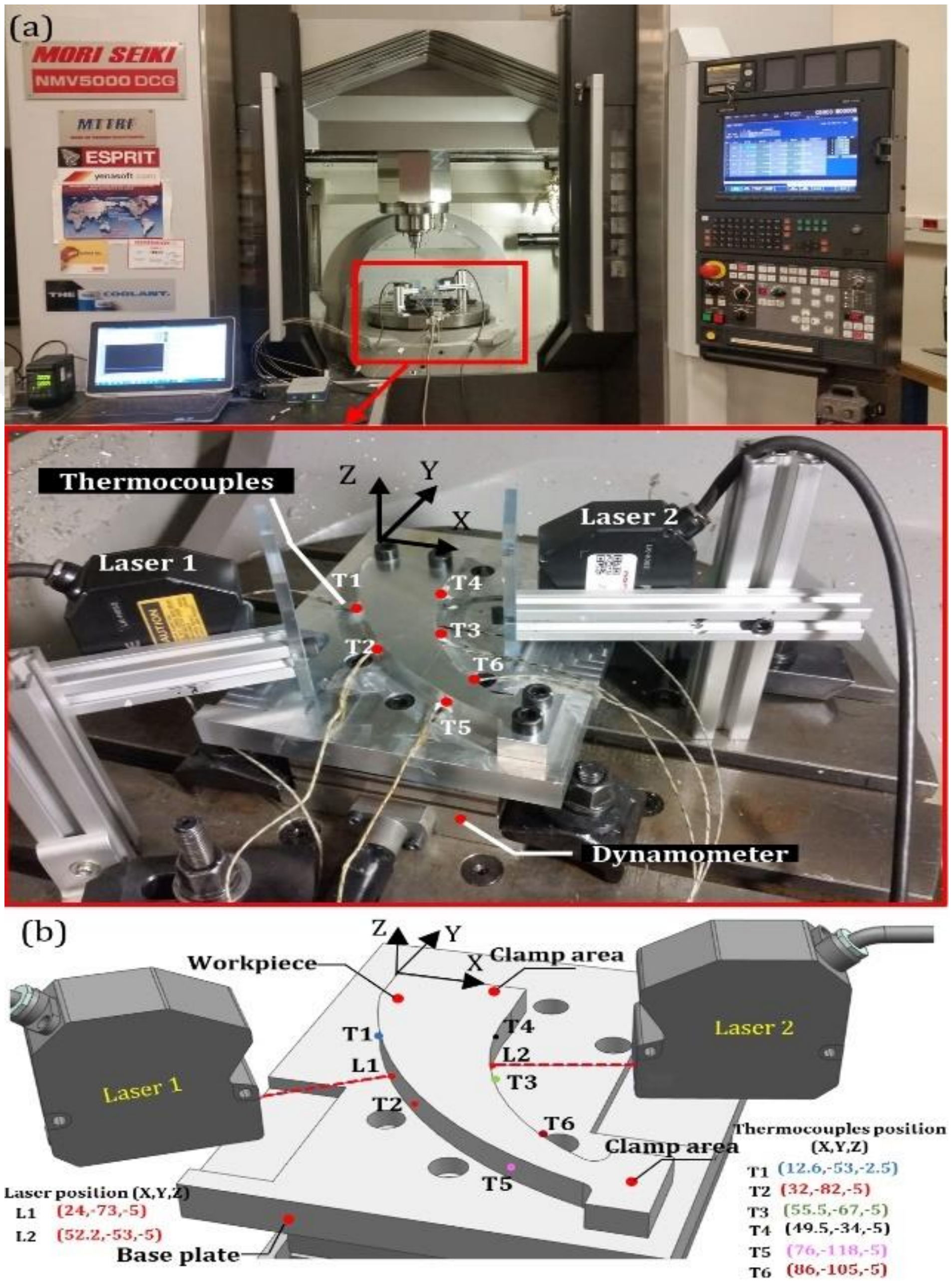

Figure 3-8: (a) Experimental setup (b) Diagram of the setup showing the locations of measurement sensors (X, Y, Z).

The force model is validated by comparing the measured cutting forces during the machining operation with the estimated forces. The comparison of the cutting forces for the first pocket and second pocket outer tool path is shown in Figure 3-9 and Figure 3-10 . It can be inferred that the simulated results show good agreement with the experiments, the trend and the magnitude of the simulated cutting force are matching well which confirms the validity of the cutting force model.

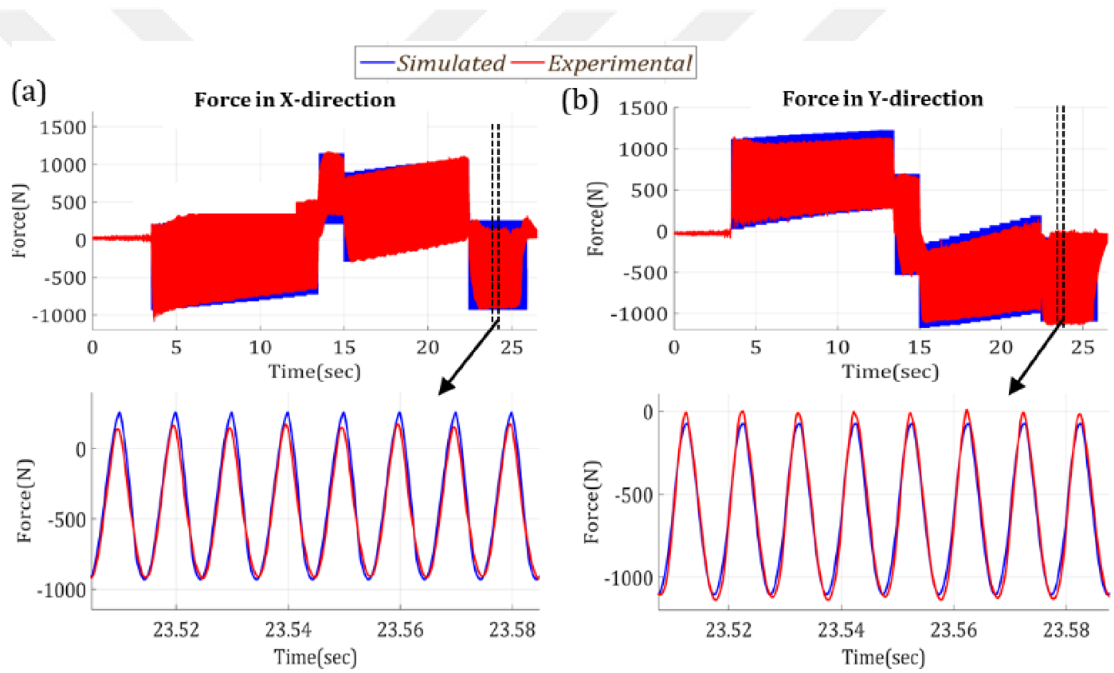

Figure 3-9: Comparison between the measured and simulated cutting forces of first pocket outer tool path and close-up views in four tool revolution; (a) cutting forces in the X direction, (b) cutting forces in the Y direction.

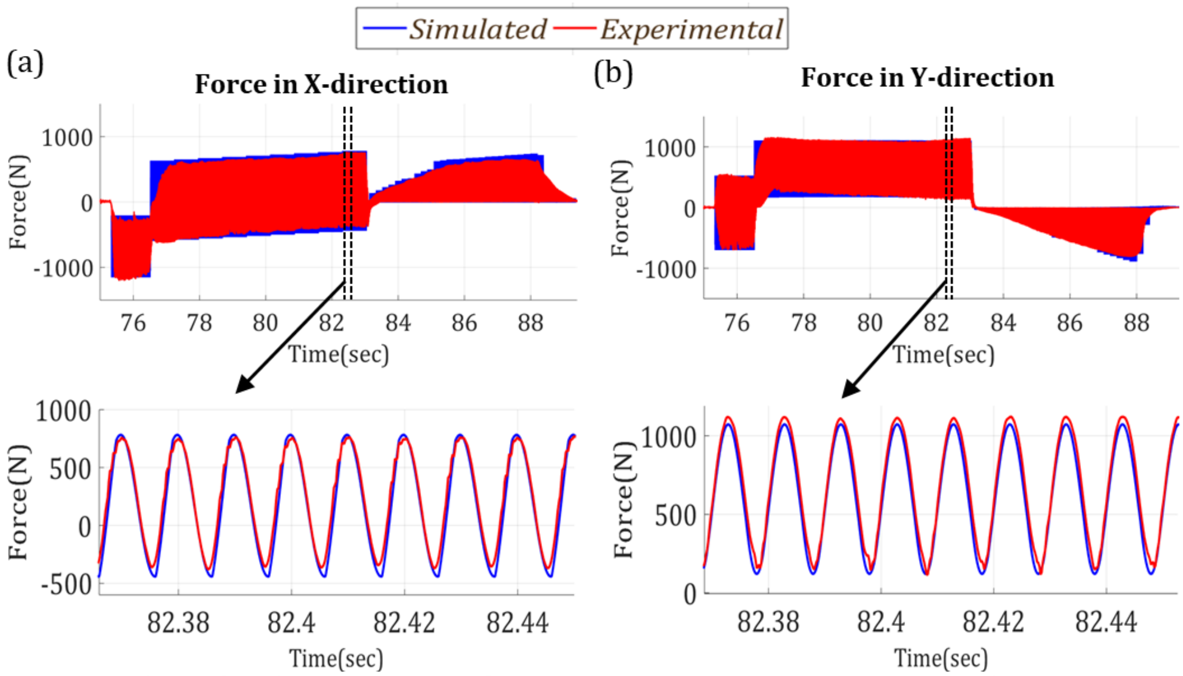

Figure 3-10: Comparison between the measured and simulated cutting forces of second pocket outer tool path and close-up views in four tool revolution; (a) cutting forces in the X direction, (b) cutting forces in the Y direction.

Similarly, the measured temperatures on the complex thin-wall geometry are compared with the simulated temperature peaks and shown in Figure 3-11. The simulated results are in a good agreement with the experiments and the model can predict the temperature with a minimum 5% to a maximum 14% error which is acceptable. The simulated temperature distribution for the first pocket and second pocket at different machining time is illustrated in Figure 3-12 and Figure 3-13.

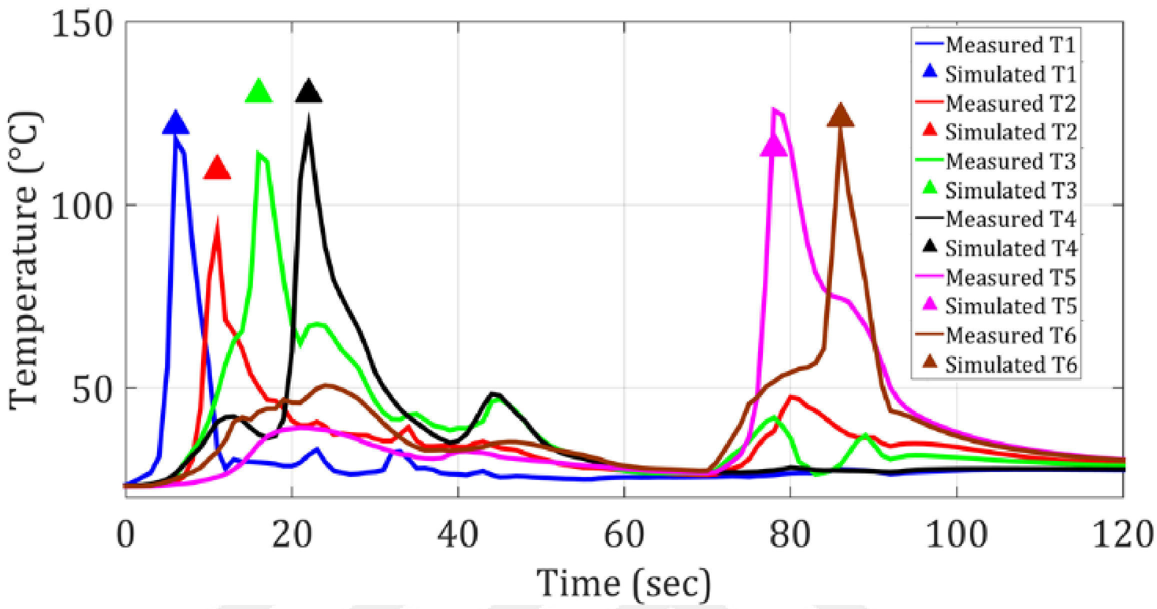

Figure 3-11: Comparison of simulated temperatures peaks and the experimental measurement.

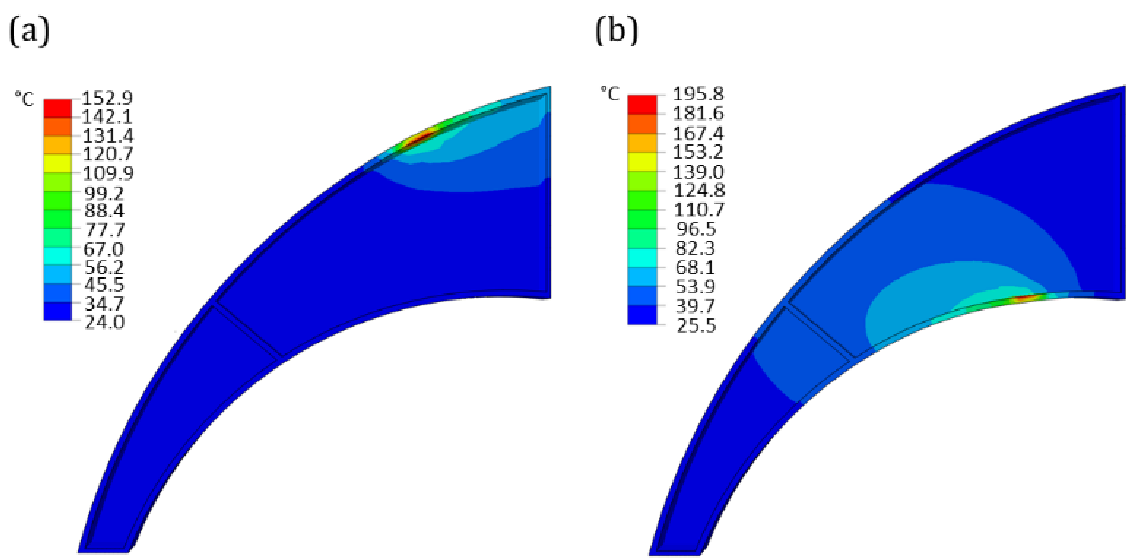

Figure 3-12: Simulated temperature distributions for first pocket at the various milling time of (a) 6.51 sec and (b) 20.65 sec.

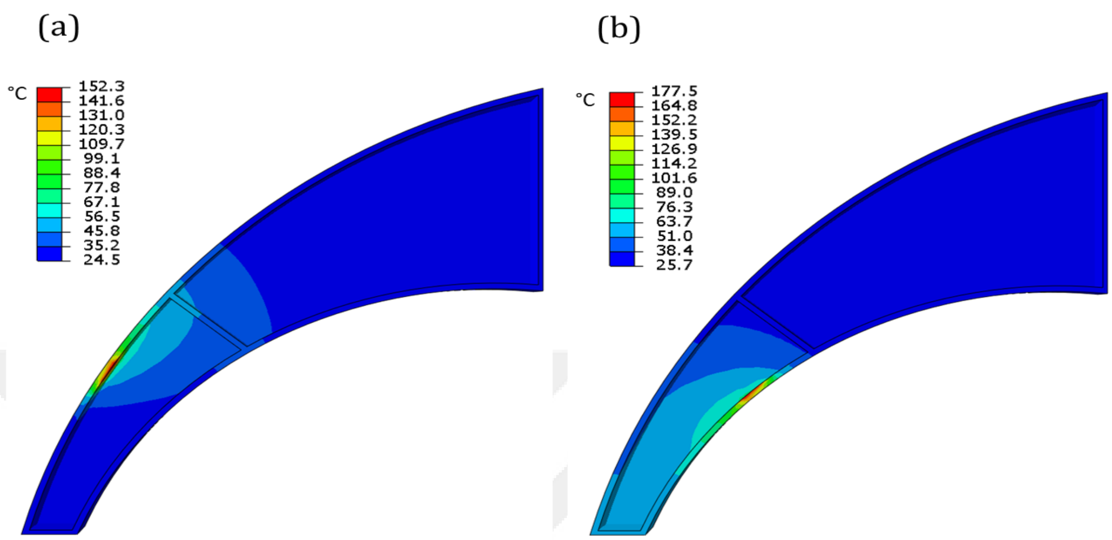

Figure 3-13: Simulated temperature distributions for second pocket at the various milling time of (a) 78.8 sec and (b) 87.6 sec.

The measured displacement with laser sensor at the L1 position and the simulated deformation for the outer tool pass for the first pocket is shown in Figure 3-14. The figure provides important information about the elastic and plastic deformation during the cutting process. As it can be inferred from the figure that the amplitude of deformation increases as the tool proceeds along the designated internal pocket path towards the laser sensor point and decreases as the tool moves away. This shows the elastic deformation of the workpiece and it recovers after the tool pass. The deformation left in the workpiece after the pass is the plastic deformation. The plastic deformation is the permanent deformation left in the workpiece. The simulated displacement profile follows the same waveform with the experimental measurement with a peak deformation error of 15%.

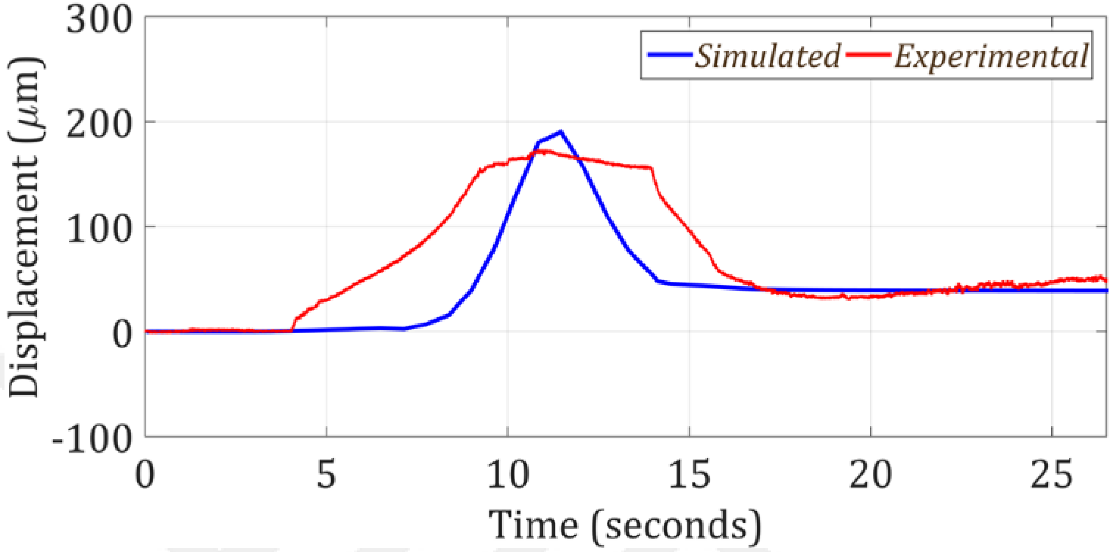

Figure 3-14: Comparison of the simulated deformation profile with the real-time deformation measurements at point L1 with laser 1 for the complete outer tool pass of the first pocket.

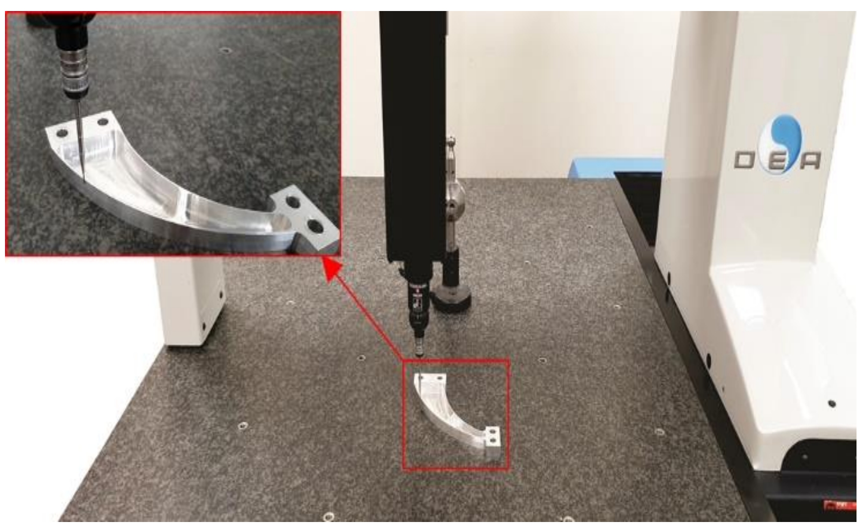

Figure 3-15: Measurement of part distortion on the coordinate measurement machine.

After the machining operation, the part is removed from the machining setup and placed on a coordinate measurement machine (CMM) to measure the final part distortion as shown in Figure 3-15. The measurement is performed on the back side of the machined wall surface from path P1 to P2 along the X-direction at 2.5 mm depth from the top surface as shown in Figure 3-16(a). The comparison between the simulated and the measured distortion profiles are shown in Figure 3-16(b). It is observed that the distortion simulation follows the experimental trend with a maximum error of 25%.

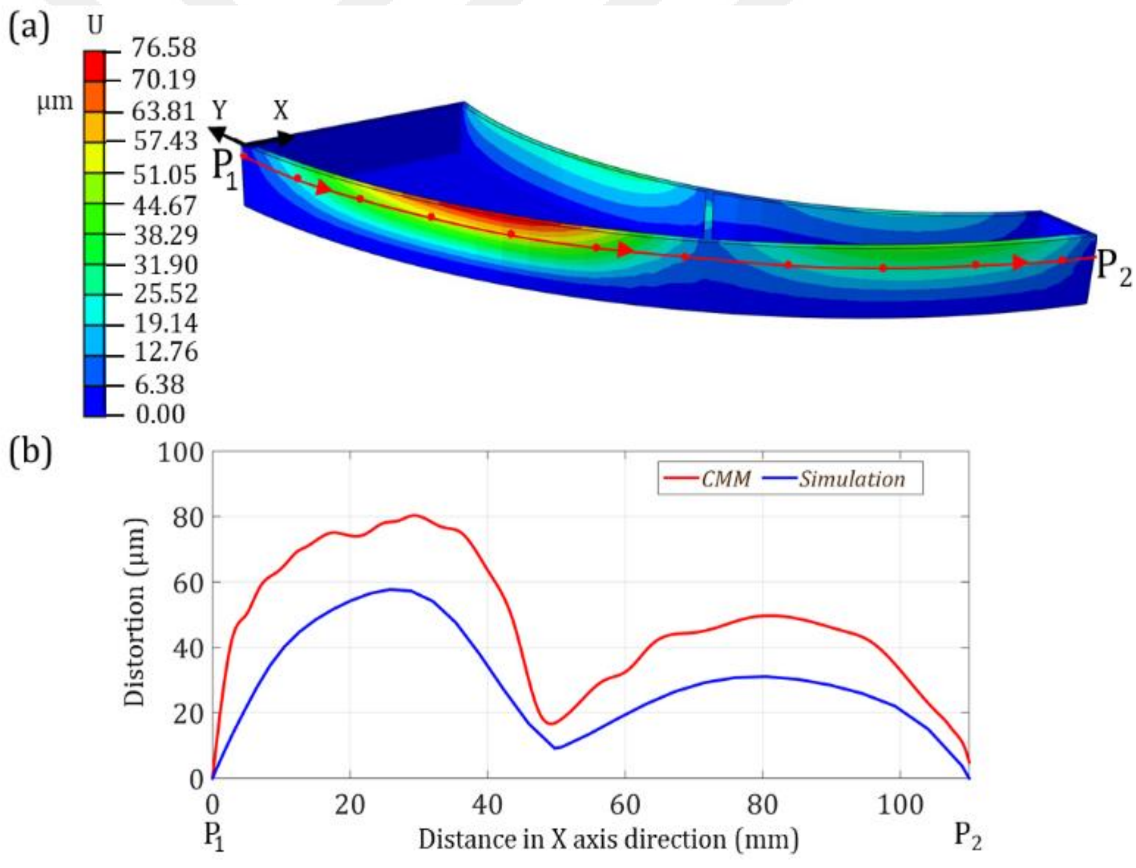

Figure 3-16: Final part distortion; (a) coordinate measurement path (P1-P2) along X-direction, and (b) comparison of the simulated and measured distortion profile with CMM.

3.5 Summary

The generation of residual stresses during the machining operation breaks the balance of the internal stress in the part. Thus, the part undergoes deformation to maintain the internal stress balance. The machined induced residual stresses are highly dependent on the cutting and thermal load which leads to the dimensional inaccuracy in the thin-wall parts.

This chapter presents the model to predict the distortion of complex thin-wall structural parts due to machining load. The combined effect of cutting load and thermal load is considered in the FEM model and distortions are estimated for Al7050 T7451 workpiece material. A new method is proposed to apply the thermo-mechanical loads to the relevant nodes in the model. The cutting and thermal loads are analytically obtained and used as an input in the model. The simulated cutting forces and temperatures are compared with the measured cutting forces and temperatures and found in a good agreement. The validity of the model is evaluated both in terms of part stability during machining with real-time laser sensor measurements and resulting part distortion with a CMM. Promising results are obtained from the validation of the simulation with the laser sensor and CMM measurements with errors as low as 15% and %25, respectively.

Chapter 4
MACHINING OF GAMMA TITANIUM ALUMINIDE

4.1 Overview

Gamma titanium aluminide (γ-TiAl) is a material of choice for aerospace and automotive applications due to its superior thermo-mechanical properties. Nevertheless, it is difficult to machine material. Although machining of γ-TiAl alloys has been previously researched in the literature, no studies have been carried out to develop an orthogonal cutting database for the prediction of cutting forces for γ-TiAl in oblique and 3D processes such as flat and ball-end milling. The creation of such a database is crucial for accurate and fast predictions of cutting forces employed in high-performance machining of aeronautic components such as blades. This implies that industrial parameters such as the surface roughness, possibility of chatter or dimensional tolerances can be accurately predicted. A fundamental cutting parameter database independent of cutter geometry is required to calculate the cutting forces in a machining operation. This database is then used to calculate the specific cutting coefficients by applying an analytical orthogonal to oblique transformation model. High-performance coatings have become a successful standard for increasing the efficiency of machining tools in the industry over the last decade.

In this chapter, the orthogonal cutting database for 48-2-2 γ-TiAl is established for different tool coatings; AlTiN and AlCrN coatings. For cutting force predictions, an analytical force model and the orthogonal to oblique transformation method is employed. The model is then validated for end milling and ball-end milling operations for different cutting conditions.

4.2 Orthogonal to oblique transformation

Orthogonal to oblique transformation is the cutter independent technique used to calculate the cutting coefficients for cutting force model. The advantage of this technique is that it can provide the cutting coefficients before tool manufacturing. This method is based on the calculation of fundamental orthogonal parameters like shear stress, shear angle and friction angle using the measured orthogonal turning force in tangential and feed direction and chip thicknesses. Transformation of these parameters is then utilized to model oblique cutting processes such as the milling operation. The fundamental parameters are calculated using the following equations:

$$\beta_a = \alpha_r + tan^{-1}\frac{F_{fc}}{F_{tc}}$$ Equation 4-1

$$\mu = tan(\beta_a)$$ Equation 4-2

$$\emptyset_c = \frac{\pi}{4} - \frac{(\beta_a - \alpha_r)}{2}$$ Equation 4-3

$$\tau_s = \frac{F\,cos(\emptyset_c + \beta_a - \alpha_r)\,sin\,\emptyset_c}{bh}$$ Equation 4-4

$$r_c = \frac{tan(\emptyset_c)}{cos(\alpha_r)((tan(\alpha_r)tan(\emptyset_c)+1)}$$ Equation 4-5

Here $\beta_a, \alpha_r, F_{fc}, F_{tc}, \mu, \emptyset_c, \tau_s, F, b, h$ and r_c are friction angle, rake angle, average feed cutting force, average tangential cutting force, the coefficient of friction, shear angle, shear stress, average resultant force, the width of cut, uncut chip thickness, and chip thickness ratio in orthogonal turning, respectively.

In order to measure the shear angle, the chip thickness measurement is required. However, due to the low ductility of γ-TiAl, the produced chips during the machining operation are expected to be discontinuous, making the deformed chip thickness measurement and empirical calculation of chip ratio challenging. To tackle this issue, the minimum energy principle is employed to estimate the shear angle as given in Equation 5-

4. This model assumes that the shear stress on the shear plane is equivalent to the yield shear stress of the material and that the shear plane is thin [85].

The cutting coefficient for milling operation utilized in this chapter are calculated using orthogonal to oblique transformation method [82] and are shown in the following equations:

$$K_{tc} = \frac{\tau_S}{\sin \emptyset_n} \frac{\cos(\beta_n - \alpha_n) + \tan i \tan \eta \sin \beta_n}{\sqrt{\cos^2(\emptyset_n + \beta_n - \alpha_n) + \tan^2 \eta \sin^2 \beta_n}} \quad \text{Equation 4-6}$$

$$K_{rc} = \frac{\tau_S}{\sin \emptyset_n \cos i} \frac{\sin(\beta_n - \alpha_n)}{\sqrt{\cos^2(\emptyset_n + \beta_n - \alpha_n) + \tan^2 \eta \sin^2 \beta_n}} \quad \text{Equation 4-7}$$

$$K_{ac} = \frac{\tau_S}{\sin \emptyset_n} \frac{\cos(\beta_n - \alpha_n) \tan i - \tan \eta \sin \beta_n}{\sqrt{\cos^2(\emptyset_n + \beta_n - \alpha_n) + \tan^2 \eta \sin^2 \beta_n}} \quad \text{Equation 4-8}$$

4.3 Cutting force model for ball-end mill

The ball-end milling process is widely used in the machining of free form surfaces especially in the automobile, aerospace, and die and mold industries. Therefore, the prediction of cutting forces for ball-end milling is important to optimize the tool geometry for best performance. The cutting forces for ball end milling are modeled as given [49] and reproduced here as:

$$dF_{t,j}\left(\theta_j, k(z)\right) = K_{tc} h\left(\theta_j, k(z)\right) db(z) + K_{te} dS(z) \quad \text{Equation 4-9}$$

$$dF_{r,j}\left(\theta_j, k(z)\right) = K_{rc} h\left(\theta_j, k(z)\right) db(z) + K_{re} dS(z) \quad \text{Equation 4-10}$$

$$dF_{a,j}\left(\theta_j, k(z)\right) = K_{ac} h\left(\theta_j, k(z)\right) db(z) + K_{ae} dS(z) \quad \text{Equation 4-11}$$

Here, $dF_{t,j}$, $dF_{r,j}$ and $dF_{a,j}$ are the differential tangential, radial and axial cutting force component. Similarly, $\theta_j, k(z), db(z)$ and $dS(z)$ are the angular position, axial angle, chip width and edge length in the disk j. The calculation of these parameters is shown in the following equations:

$$k(z) = \sin^{-1}\sqrt{1 - E(z)^2}\,,$$

$$dS(z) = \sqrt{tan^2 i_o(1 - E(z)^2) + \frac{1}{1 - E(z)^2}}\,, \qquad \text{Equation 4-12}$$

$$E(z) = \frac{R - z}{R} \text{ and } db = \frac{dz}{\sin k(z)}$$

Here, dz , i_o and R represents the axial integration element, the nominal helix angle and the tool radius.

The differential cutting forces in the cartesian coordinates are obtained with the following relation:

$$\begin{bmatrix} dF_{x,j} \\ dF_{y,j} \\ dF_{z,j} \end{bmatrix} = \begin{bmatrix} -sin(k)\,sin(\theta_j) & -cos(\theta_j) & -\cos(k)\sin(\theta_j) \\ -sin(k)\,cos(\theta_j) & sin(\theta_j) & -\cos(k)\cos(\theta_j) \\ cos(k) & 0 & -sin(k) \end{bmatrix} \times \begin{bmatrix} dF_{r,j} \\ dF_{t,j} \\ dF_{a,j} \end{bmatrix} \qquad \text{Equation 4-13}$$

The total cutting forces in the X, Y and Z direction can be predicted by the summation of all cutting edge forces as shown:

$$F = \sum_{j=1}^{N}\sum_{z1}^{z2} F_j\,(\theta_j) \qquad \text{Equation 4-14}$$

Above, N is the total number of cutting edges and z1 and z2 represent the lower and upper limit of the discretized cutting edge.

Owing to the geometry of the ball-end milling tool, the engagement area doesn’t remain constant and the complete cutting-edge length is not in contact with the workpiece during the freeform surface machining. In this study, the cutting forces for freeform ball-end milling are predicted by employing a solid modeler-based engagement model to predict the contact region between the tool and the workpiece. First, the contact surface between the tool and the workpiece is calculated at each cutter location, then the swept volume of the cutting tool is calculated from the cutter location (CL) file. The entrance and exit angles of each discrete cutting disc are calculated after subtracting the swept volume from a blank workpiece. These angles are used as an input for the force model. A detailed explanation of the employed engagement model is provided in [86]. A sample contact region for a given cutter location on a freeform milling surface is shown in Figure 4-1.

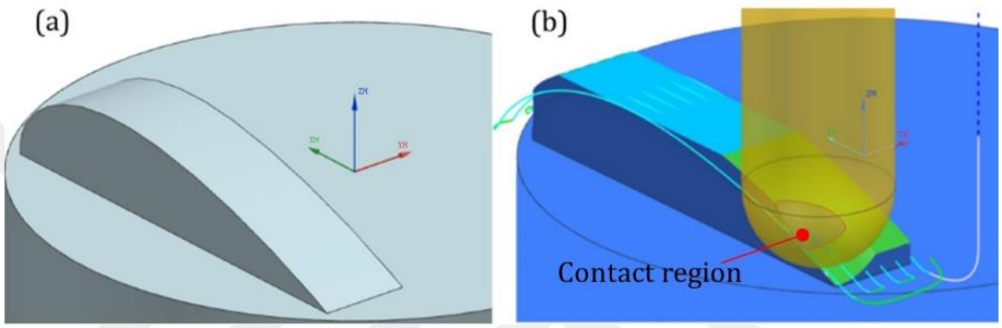

Figure 4-1: (a) CAD model of the freeform surface, (b) CAM simulation and tool-workpiece contact region.

4.4 Experimental setup

The experimental setup consists of both orthogonal turning and milling of 48-2-2 γ-TiAl, a difficult to cut material. The orthogonal database is established by performing orthogonal turning test, whereas the milling tests are conducted to validate the predicted cutting forces obtained from the developed database.

4.4.1 Orthogonal turning setup

Orthogonal cutting tests are performed on a Mazak Quick Turn Nexus 150 turning center as shown in Figure 4-2(a). A grooved 48-2-2 γ-TiAl workpiece with 55 mm diameter and 2 mm width of cut is used during tests. The inclination angle is set to zero degrees to have an orthogonal cutting condition. All experimental tests are performed for 40 m/min cutting speed and 0.06,0.08 and 0.100 mm/rev feedrates. Cutting operations are conducted with a 4° rake angle and tungsten carbide inserts with two different coatings: AlCrN and AlTiN coatings. No coolant is used during the machining and cutting forces are measured using Kistler 9257B table type dynamometer.

4.4.2 Milling setup

A set of experimental tests consisting of flat and ball-end milling are performed on a 5-axis Mori Seiki NMV5000 DCG machining center as shown in Figure 4-2(b). Once again, all the milling tests are conducted at dry conditions and a Kistler 9257B table type dynamometer is utilized for cutting force data collection.

Flat end milling tests are conducted with 36.5° helix angle, 8° rake angle, 12 mm diameter, four fluted tungsten carbide end mills having two different coating conditions: AlCrN and AlTiN coating. The thicknesses of the coatings are measured using a scanning electron microscope (SEM) shown in Figure 4-3. Cutting force data is acquired during down milling operation for the tool path shown in Figure 4-4. The cutting conditions are tabulated in Table 4-1.

The estimated cutting forces for ball-end milling are validated by performing down end milling and freeform surface milling using AlCrN coated, four fluted, tungsten carbide ball-end mill with 30° nominal helix angle, 8 mm nominal diameter, and 5° rake angle. The cutting conditions are tabulated in Table 4-2 and Table 4-3. The cutting tools used in the study are shown in Figure 4-5.

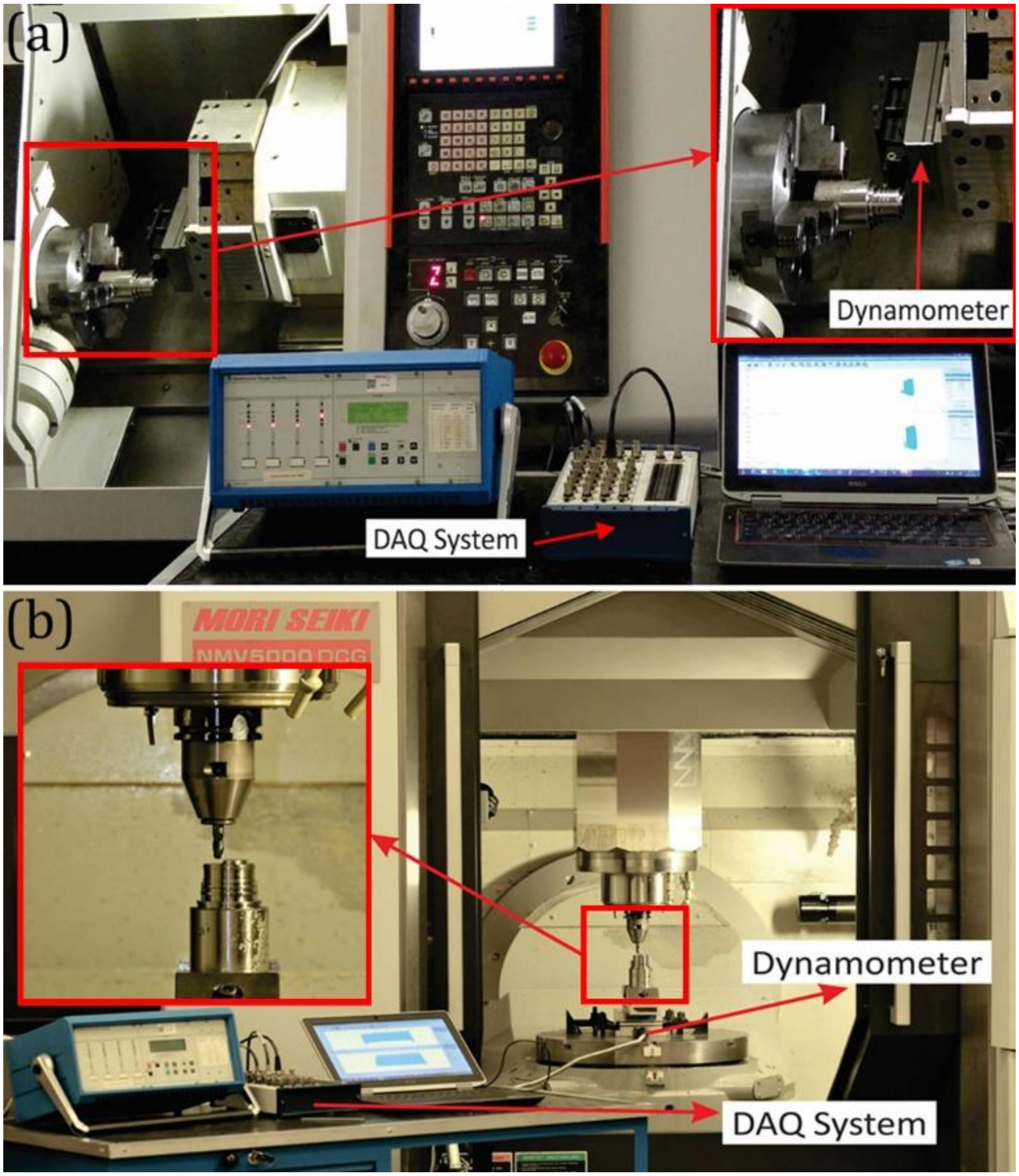

Figure 4-2: (a) Orthogonal turning setup for 48-2-2 γ-TiAl machining, (b) Milling test setup for 48-2-2 γ-TiAl machining.

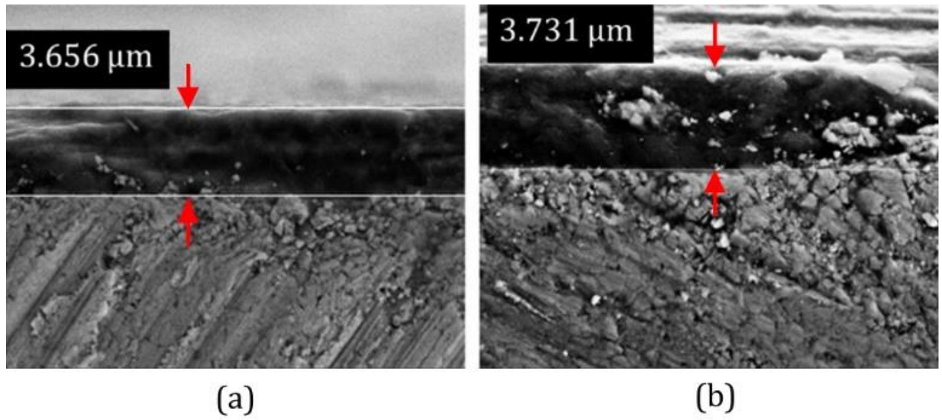

Figure 4-3: Flat end mill coating thickness; (a) AlCrN coating, (b) AlTiN coating.

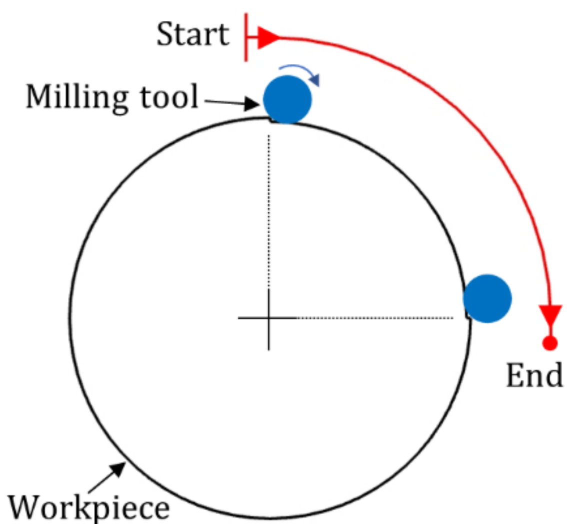

Figure 4-4: Toolpath for flat end milling.

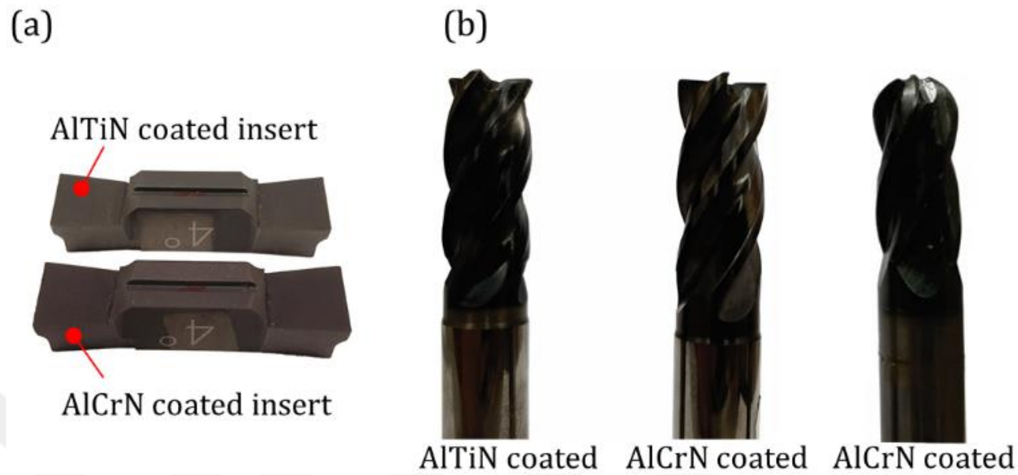

Figure 4-5: Cutting tools used in the experiments; (a) coated turning inserts, (b) coated end mills and ball-end mill.

Table 4-1: Flat end milling cutting conditions for 48 2-2 γ-TiAl.

Cutting speed [m/min]	Depth of cut [mm]	Width of cut [mm]	Feedrate [mm/min]
15	2	0.5	64, 84, 112, 128

Table 4-2: Ball-end milling cutting conditions for 48 2-2 γ-TiAl in down end milling.

Cutting speed [m/min]	Depth of cut [mm]	Width of cut [mm]	Feedrate [mm/min]
48	3	0.5	336, 480, 624

Table 4-3: Ball-end milling cutting conditions for 48 2-2 γ-TiAl in freeform milling.

Cutting speed [m/min]	Stepover [mm]	Feedrate [mm/min]
40	1	576

4.5 Results and discussion

4.5.1 Orthogonal turning of 48-2-2 γ-TiAl

The measured tangential and feed forces from orthogonal turning for different feedrates are shown in Figure 4-6. The fundamental cutting parameters such as shear stress, shear angle, friction angle and chip ratio are calculated using the measured tangential and feed force. The equations mentioned in section 5.2 are used to calculate these parameters. The calculated orthogonal cutting parameters for different coatings are tabulated in Table 4-4 for 4° rake angle.

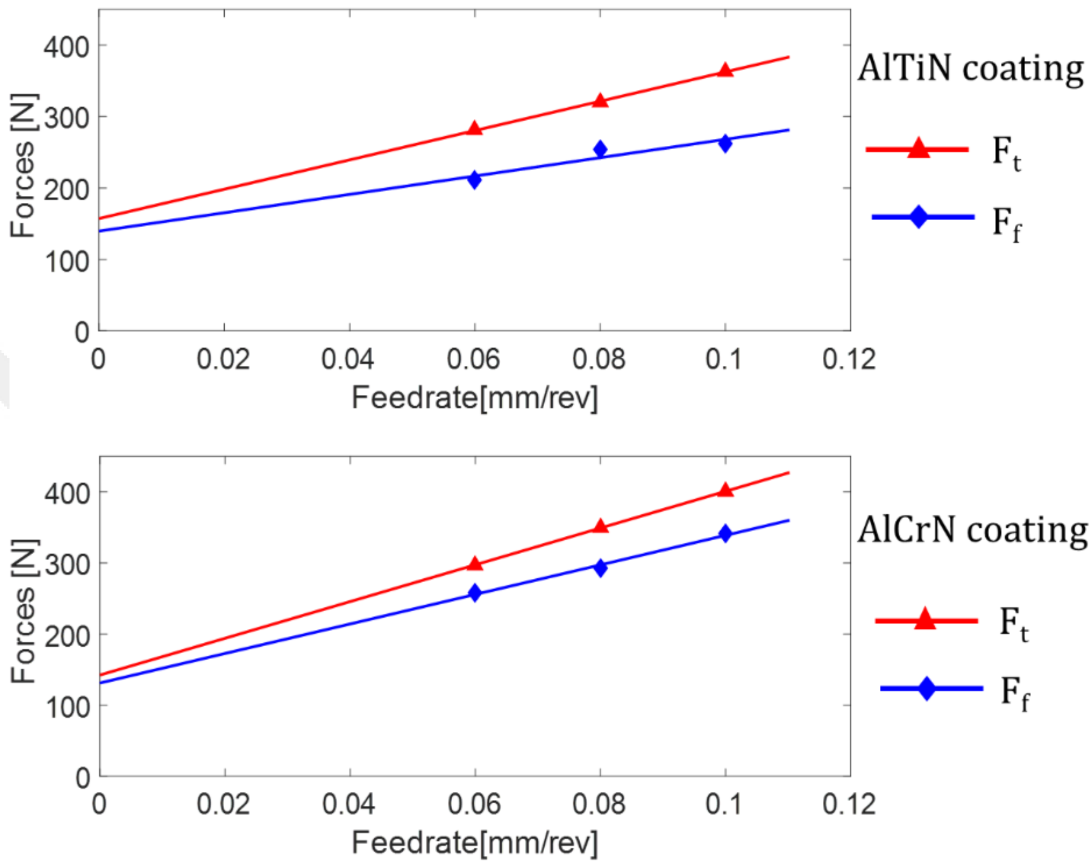

Figure 4-6: Comparison of measured cutting forces in the orthogonal turning of 48 2-2 γ-TiAl for 4° rake angle and different coatings.

Table 4-4: Orthogonal to oblique database for 48 2-2 γ-TiAl.

Parameters	AlTiN	AlCrN
Chip ratio (r_c)	0.54	0.46
Friction angle (β_a)	35.6°	42.6°
Friction coefficient (μ)	0.72	0.92
Shear angle ($\emptyset_c$)	29.2°	25.7°
Shear stress (τ_s)	289.1 MPa	311.5 MPa
K_{te}	78 N/mm	71 N/mm
K_{re}	70 N/mm	66 N/mm

Results show that the AlCrN coating has a smaller shear angle as compared to the AlTiN coating. In the cutting process, the chip thickness, shear angle and shear plane are interrelated to each other. A smaller shear angle is associated with a longer shear plane and a relatively large chip thickness. On the other hand, a large shear angle indicates a small shear plane and during the cutting process, produced chips are relatively thinner [87]. This results in less force needed to shear off the chips, implying that a lower friction coefficient dictates the process.

Friction coefficient plays an important role in the tool life and workpiece integrity [88]. Friction coefficient identified from the orthogonal turning shows that the AlCrN coating has the highest friction coefficient as compared to the AlTiN coating. No significant change in shear stress is observed by changing the coatings.

4.5.2 Flat end milling of 48-2-2 γ-TiAl

The cutting forces for end milling operation are simulated using the analytical model presented in section 3.2.1. To model the cutting forces, the cutting coefficients are determined using the orthogonal to oblique transformation technique. The calculated edge cutting coefficients from orthogonal force data are shown in Table 4-4. The estimated and measured resultant cutting forces for flat end milling for different coatings and feedrates are compared in Figure 4-7 and Figure 4-8. It can be inferred from these figures that the suggested force model is able to predict the resultant cutting forces within 13% error band for AlCrN coated tools and 20% error band for AlTiN coated tools, which confirms the validity of the force model for different coatings.

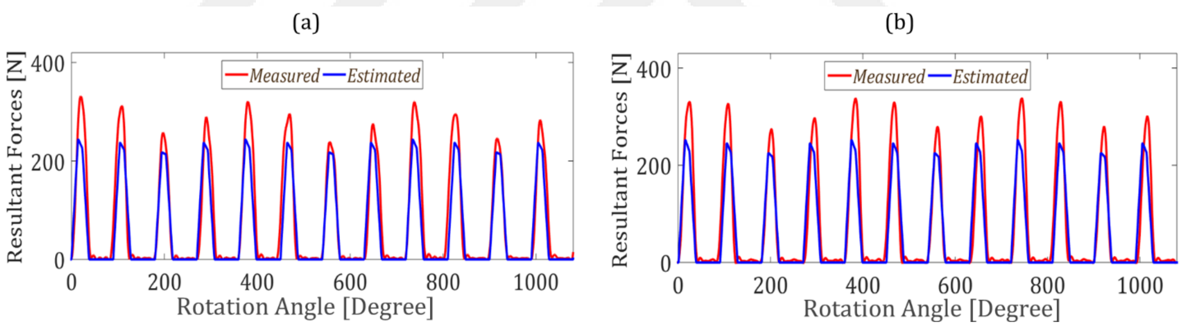

Figure 4-7: Measured and estimated resultant cutting forces for AlTiN coated tool for flat end down-milling; (a) feedrate of 64 mm/min, (b) feedrate of 88 mm/min.

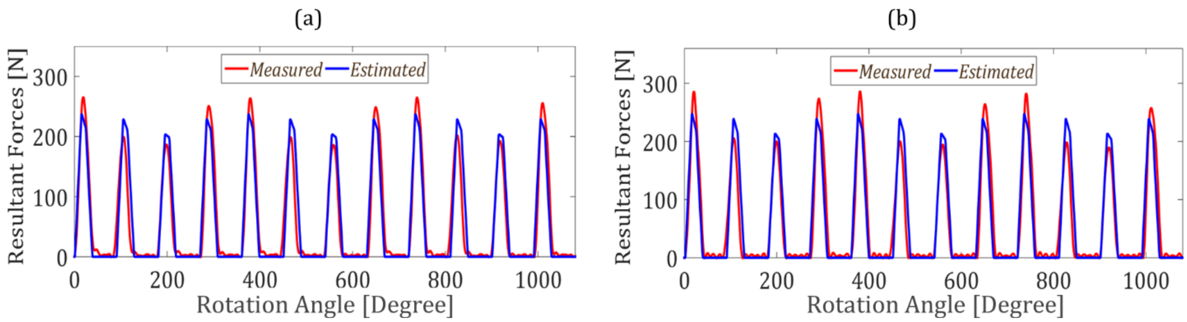

Figure 4-8: Measured and estimated resultant cutting forces for AlCrN coated tool for flat end down-milling; (a) feedrate of 64 mm/min, (b) feedrate of 88 mm/min.

4.5.3 Ball-end milling of 48-2-2 γ-TiAl

Down end milling operations are performed using two different engagement conditions as shown in Figure 4-9. Comparison between the simulation and the experimental data for these engagement conditions are shown in Figure 4-10 and Figure 4-11; validation tests show that the simulated and measured cutting forces match well within 15% error band.

NACA 2429 airfoil profile is machined to validate the accuracy of orthogonal parameters for 48-2-2 γ-TiAl on freeform surfaces as shown in Figure 4-12. The machining is performed in 4 layers with 6 paths in each layer. Estimated and measured cutting forces in the X and Y directions for the third path in the fourth layer are shown in Figure 4-13. It can be inferred that the trend and the magnitude of the simulated and experimental cutting forces are in good agreement. The deviation in the cutting forces can be attributed to the instabilities that occur during machining operations.

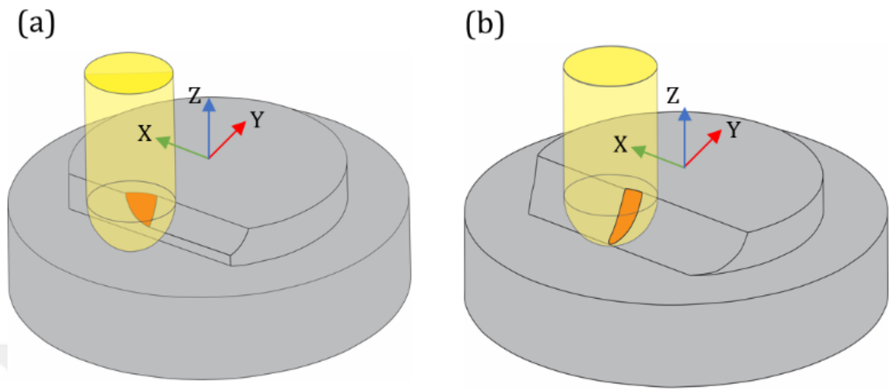

Figure 4-9: Ball-end milling engagement area; (a) 4th pass down milling, (b) 6th pass down milling.

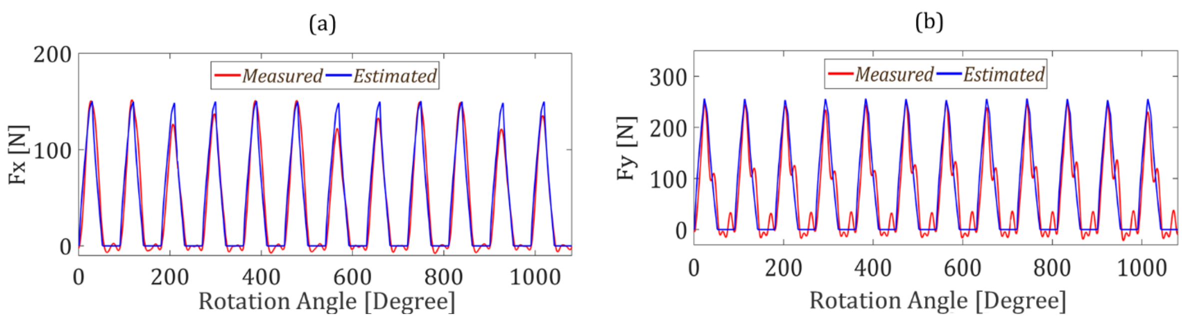

Figure 4-10: Comparison between the measured and estimated cutting forces for 4th pass down-milling with the feedrate of 480 [mm/min]: (a) cutting forces in the X direction, (b) cutting forces in the Y direction.

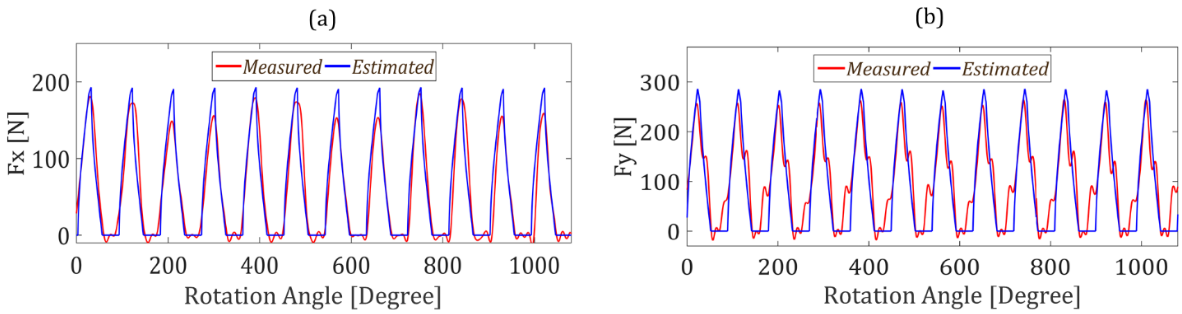

Figure 4-11: Comparison between the measured and estimated cutting forces for 6th pass down-milling with the feedrate of 480 [mm/min]: (a) cutting forces in the X direction, (b) cutting forces in the Y direction.

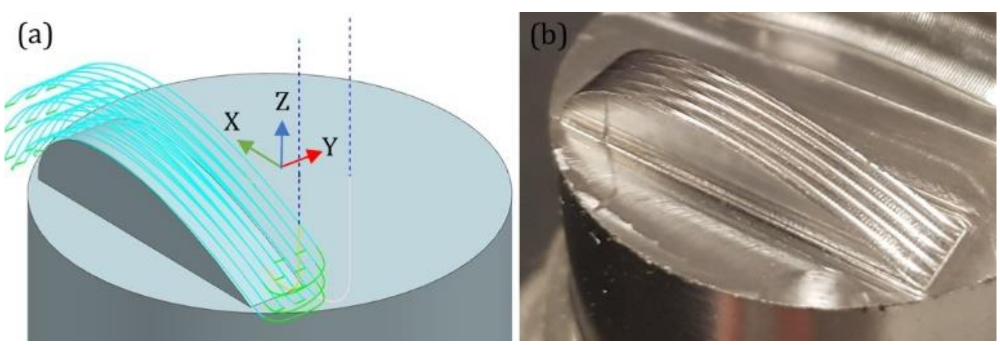

Figure 4-12: (a) Cutting tool path for an airfoil geometry, (b) Machined part.

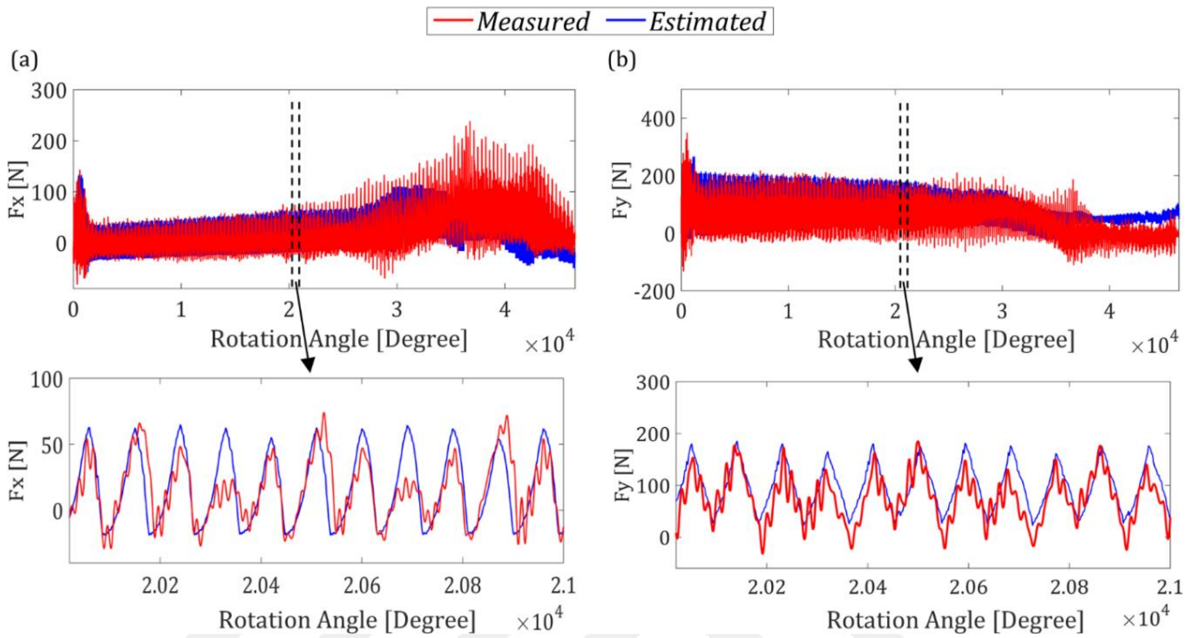

Figure 4-13: Comparison between the measured and estimated cutting forces of 4th layer, 3rd tool pass with 576 [mm/min] feedrate; close-up view for cutting forces in (a) the X direction and (b) the Y direction.

4.6 Chip morphology

The chip morphology observation during the turning and milling operation confirms a serrated, discontinuous and segmented chip geometry for all the cutting conditions. This phenomenon is due to the brittleness and low fracture toughness of γ-TiAl. Figure 4-14 represents the chip morphology in the orthogonal turning and milling processes.

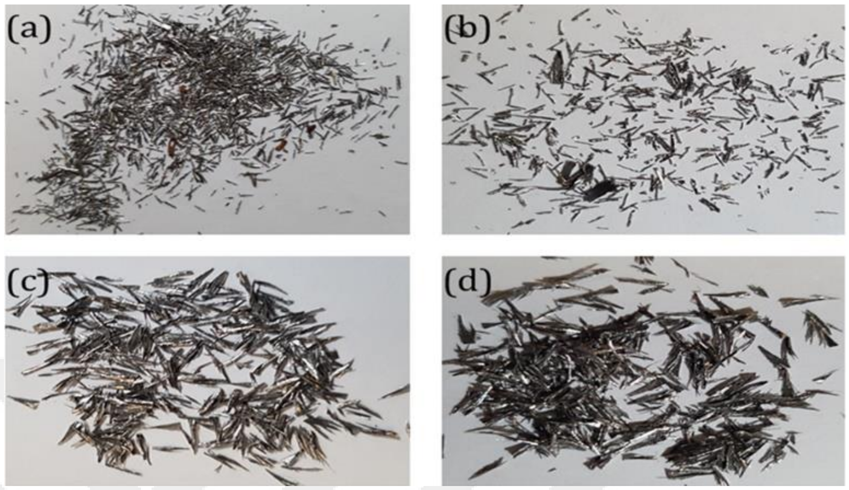

Figure 4-14: Chip morphology of 48-2-2 γ-TiAl; in orthogonal turning at (a) 0.08 mm feedrate, (b) 0.100 mm feedrate, and in ball-end milling at (c) 336 mm/min feedrate, (d) 480 mm/min feedrate.

4.7 Summary

In this chapter, an orthogonal database for 48-2-2 γ-TiAl is established to predict the fundamental cutting parameters. The effect of coating on friction coefficient, shear stress, shear angle and cutting forces are also investigated. It is found that the shear angle for AlCrN coated tool is less than the AlTiN coated tool, whereas the friction coefficient for the AlCrN coated tool is observed to be greater than the AlTiN coated tool. The developed database is employed to predict the cutting forces of 48-2-2 γ-TiAl for milling operation using analytical force model. Estimated cutting forces, validated via end milling experiments, are found within 13% and 20% error band for AlCrN and AlTiN coatings, whereas cutting forces validated via ball-end milling experiments match well within 15% error band for AlCrN coating. This study aims to be an important guide for machining of 48 2-2 γ-TiAl alloys and facilitating the transition from processing traditional materials to advanced materials for manufacturing industries.

BIBLIOGRAPHY

[1] D. Chantzis, S. Van-Der-Veen, J. Zettler, W.M. Sim, An industrial workflow to minimise part distortion for machining of large monolithic components in aerospace industry, Procedia CIRP. 8 (2013) 281–286. doi:10.1016/j.procir.2013.06.103.

[2] Kaiser Aluminum, (n.d.). http://www.kaiseraluminum.com/ (accessed May 21, 2019).

[3] Lusina - Usinage pièce grande dimension et surfaçage, (n.d.). http://www.lusina.eu/ (accessed May 21, 2019).

[4] K. Ma, R. Goetz, Modeling of Residual Stress and Machining Distortion in Aerospace Components, Metals Process Simulation. (2018) 386–407. doi:10.31399/asm.hb.v22b.a0005537.

[5] F. Klocke, D. Lung, M. Arft, P.C. Priarone, L. Settineri, On high-speed turning of a third-generation gamma titanium aluminide, International Journal of Advanced Manufacturing Technology. 65 (2013) 155–163. doi:10.1007/s00170-012-4157-5.

[6] G.T. Smith, CNC Machining Technology: Volume 3: Part Programming Techniques, Springer London, 2013. https://books.google.com.tr/books?id=VdPiBwAAQBAJ.

[7] X.W. Xu, S.T. Newman, Making CNC machine tools more open, interoperable and intelligent - A review of the technologies, Computers in Industry. 57 (2006) 141–152. doi:10.1016/j.compind.2005.06.002.

[8] J.A.C. Bokhorst, J. Slomp, N.C. Suresh, An integrated model for part-operation allocation and investments in CNC technology, International Journal of Production Economics. 75 (2002) 267–285. doi:10.1016/S0925-5273(01)00118-9.

[9] M. Safaieh, A. Nassehi, S.T. Newman, A Novel Methodology for Cross-technology Interoperability in CNC Machining, Robot. Comput.-Integr. Manuf. 29 (2013) 79–87. doi:10.1016/j.rcim.2012.04.016.

[10] Y. Altintas, P. Kersting, D. Biermann, E. Budak, B. Denkena, I. Lazoglu, Virtual process systems for part machining operations, CIRP Annals - Manufacturing Technology. 63 (2014) 585–605. doi:10.1016/j.cirp.2014.05.007.

[11] J.E. Hatch, A.S. for Metals, A.A. (U.S.), Aluminum : properties and physical metallurgy, Metals Park, Ohio : American Society for Metals, 1984. http://books.google.com/books?id=zPBRAAAAMAAJ.

[12] L.P. Troeger, E.A.S. Jr, Microstructural and mechanical characterization of a superplastic 6xxx aluminum alloy, 277 (2000) 102–113.

[13] M.C.S. Jr, A.R. Machado, W.F. Sales, Machining of aluminum alloys : a review Machining of aluminum alloys : a review, (2016). doi:10.1007/s00170-016-8431-9.

[14] F.C. Campbell, Manufacturing Technology for Aerospace Structural Materials, Elsevier Science, 2011. https://books.google.com.tr/books?id=R7NHvVJf_ZEC.

[15] E.A. Starke, J.T. Staley, Application of modern aluminum alloys to aircraft, Progress in Aerospace Sciences. 32 (1996) 131–172. doi:https://doi.org/10.1016/0376-0421(95)00004-6.

[16] C. Leyens, M. Peters, Titanium and Titanium Alloys: Fundamentals and Applications, Wiley, 2003. https://books.google.com.tr/books?id=68mQLz7yJ8UC.

[17] Application and Features of Titanium for the Aerospace Industry, n.d. https://www.nipponsteel.com/en/tech/report/nssmc/pdf/106-05.pdf (accessed June 30, 2019).

[18] F.H. Froes, Titanium: Physical Metallurgy, Processing, and Applications, A S M International, 2015. https://books.google.com.tr/books?id=WzJ7CgAAQBAJ.

[19] J.P. Davim, Machining of Titanium Alloys, Springer Berlin Heidelberg, 2014. https://books.google.com.tr/books?id=hG71AwAAQBAJ.

[20] C.T. Liu, Recent advances in ordered intermetallics, Mater. Chemi. Physics 42. 42 (1995) 77–86.

[21] B.P. Bewlay, S. Nag, A. Suzuki, M.J. Weimer, B.P. Bewlay, S. Nag, A. Suzuki, M.J. Weimer, TiAl alloys in commercial aircraft engines, Materials at High Temperatures. 3409 (2016). doi:10.1080/09603409.2016.1183068.

[22] J. Lapin, TiAl-Based Alloys : Present Status and Future, Hradec Nad Moravici. (2009)1–12. http://metal2013.tanger.cz/files/proceedings/metal_09/Lists/Papers/077.pdf.

[23] Y. Kim, Ordered Intermetallic Alloys , Part III : Gamma Titanium Aluminides, (1994).

[24] M.E. Merchant, Mechanics of the Metal Cutting Process. II. Plasticity Conditions in Orthogonal Cutting, Journal of Applied Physics. 16 (1945) 318–324. doi:10.1063/1.1707596.

[25] E.H. Lee, B.W. Shaffer, B. University., D. of A. Mathematics., U. States., O. of N. Research., U. States., N. Department., B. of Ships., The theory of plasticity applied to a problem of machining, Division of Applied Mathematics, Brown, Providence, R.I., 1949.

[26] P.L.B. Oxley, The mechanics of machining: an analytical approach to assessing machinability, E. Horwood, 1989. https://books.google.com.tr/books?id=8dhSAAAAMAAJ.

[27] A. Markopoulos, Finite Element Method in Machining Processes, 2012. doi:10.1007/978-1-4471-4330-7.

[28] D.I. Lalwani, N.K. Mehta, P.K. Jain, Journal of Materials Processing Technology Extension of Oxley ' s predictive machining theory for Johnson and Cook flow stress model, 209 (2009) 5305–5312. doi:10.1016/j.jmatprotec.2009.03.020.

[29] L. Illoul, P. Lorong, On some aspects of the CNEM implementation in 3D in order to simulate high speed machining or shearing, Computers and Structures. 89 (2011) 940–958. doi:10.1016/j.compstruc.2011.01.018.

[30] T. Ozel, I. Llanos, J. Soriano, P.J. Arrazola, 3d finite element modelling of chip formation process for machining inconel 718: Comparison of FE software predictions, Machining Science and Technology. 15 (2011) 21–46. doi:10.1080/10910344.2011.557950.

[31] M. Calamaz, J. Limido, M. Nouari, C. Espinosa, D. Coupard, M. Salaün, F. Girot, R. Chieragatti, Toward a better understanding of tool wear effect through a comparison between experiments and SPH numerical modelling of machining hard materials, International Journal of Refractory Metals and Hard Materials. 27 (2009) 595–604. doi:10.1016/j.ijrmhm.2008.09.005.

[32] M.R. Movahhedy, M.S. Gadala, Y. Altintas, Simulation of chip formation in orthogonal metal cutting process: an ALE finite element approach, Machining Science and Technology. 4 (2000) 15–42. doi:10.1080/10940340008945698.

[33] J.F. 1 T. Schermann, J. Marsolek, C. Schmidt1, Aspects of the simulation of a cutting process with ABAQUS / Explicit including the interaction between the cutting process and the dynamic behavior of the machine tool, (2006). Proceedings of 9th CIRP International Workshop on Modeling of Machining Operations .

[34] P.J. Arrazola, T. Özel, Investigations on the effects of friction modeling in finite element simulation of machining, International Journal of Mechanical Sciences. 52 (2010) 31–42. doi:10.1016/j.ijmecsci.2009.10.001.

[35] P.J. Arrazola, T. Özel, D. Umbrello, M. Davies, I.S. Jawahir, Recent advances in modelling of metal machining processes, CIRP Annals - Manufacturing Technology. 62 (2013) 695–718. doi:10.1016/j.cirp.2013.05.006.

[36] H.J. Fu, R.E. DeVor, S.G. Kapoor, A Mechanistic Model for the Prediction of the Force System in Face Milling Operations, Journal of Engineering for Industry. 106 (1984) 81–88. http://dx.doi.org/10.1115/1.3185915.

[37] J.W. Sutherland, R.E. DeVor, An Improved Method for Cutting Force and Surface

Error Prediction in Flexible End Milling Systems, Journal of Engineering for Industry. 108 (1986) 269–279. http://dx.doi.org/10.1115/1.3187077.

[38] Y. Altintaş, E. Budak, Analytical Prediction of Stability Lobes in Milling, CIRP Annals - Manufacturing Technology. 44 (1995) 357–362. doi:10.1016/S0007-8506(07)62342-7.

[39] Y. Altıntaş, P. Lee, Mechanics and Dynamics of Ball End Milling, Journal of Manufacturing Science and Engineering. 120 (2008) 684. doi:10.1115/1.2830207.

[40] H.T. Young, P. Mathew, P.L.B. Oxley, Predicting cutting forces in face milling, International Journal of Machine Tools and Manufacture. 34 (1994) 771–783. doi:10.1016/0890-6955(94)90058-2.

[41] Y. Altintas, S. Engin, Generalized modeling of milling mechanics and dynamics of milling cutters, CIRP Annals. 50 (2001) 25–30. doi.org/10.1016/S0007-8506(07)62063-0.

[42] H.Z. Li, W.B. Zhang, X.P. Li, Modelling of cutting forces in helical end milling using a predictive machining theory, International Journal of Mechanical Sciences. 43 (2001) 1711–1730. doi:10.1016/S0020-7403(01)00020-0.

[43] I. Lazoglu, S.Y. Liang, Analytical modeling of force system in ball-end milling, Machining Science and Technology. 1 (1997) 219–234. doi:10.1080/10940349708945648.

[44] E. Budak, Y. Altintaş, E.J.A. Armarego, Prediction of Milling Force Coefficients From Orthogonal Cutting Data, Journal of Manufacturing Science and Engineering. 118 (1996) 216–224. doi:10.1115/1.2831014.

[45] I. Lazoglu, Sculpture surface machining: A generalized model of ball-end milling force system, International Journal of Machine Tools and Manufacture. 43 (2003) 453–462. doi:10.1016/S0890-6955(02)00302-4.

[46] T. Altan, T. Ozel, Process simulation using finite element method — prediction of

cutting forces , tool stresses and temperatures in high- speed flat end milling, International Journal of Machine Tools and Manufacture, 40 (2000) 713–738. doi.org/10.1016/S0890-6955(99)00080-2

[47] K. Mehdi, A. Zghal, Numerical Model for Prediction of Cutting Force in Peripheral Milling Process Including Thrust and Tangential Damping Kamel MEHDI, Materials, Advanced Publications, Trans Tech. 223 (2011) 122–132. doi:10.4028/www.scientific.net/AMR.223.122.

[48] P. Lee, Y. Altintaş, Prediction of ball-end milling forces from orthogonal cutting data, International Journal of Machine Tools and Manufacture. 36 (1996) 1059–1072. doi:10.1016/0890-6955(95)00081-X.

[49] J. Gradišek, M. Kalveram, K. Weinert, Mechanistic identification of specific force coefficients for a general end mill, International Journal of Machine Tools and Manufacture. 44 (2004) 401–414. doi:10.1016/j.ijmachtools.2003.10.001.

[50] Z.Q. Yao, X.G. Liang, L. Luo, J. Hu, A chatter free calibration method for determining cutter runout and cutting force coefficients in ball-end milling, Journal of Materials Processing Technology. 213 (2013) 1575–1587. doi:10.1016/j.jmatprotec.2013.03.023.

[51] S.E. Layegh K, I. Lazoglu, A new identification method of specific cutting coefficients for ball end milling, Procedia CIRP. 14 (2014) 182–187. doi:10.1016/j.procir.2014.03.059.

[52] H. El-Hofy, Fundamentals of Machining Processes: Conventional and Nonconventional Processes, 2006. doi:10.1201/9780429443329.

[53] D.A. Stephenson, john S. Agapiou, Metal Cutting Theory and Practice, CRC Press, Taylor & Francis Group, 2005.

[54] S.W. Kim, C.M. Lee, D.W. Lee, J.S. Kim, Y.H. Jung, Evaluation of the thermal characteristics in high-speed ball-end milling, Journal of Materials Processing

Technology. 113 (2001) 406–409. doi:10.1016/S0924-0136(01)00713-0.

[55] C. Ming, S. Fanghong, W. Haili, Y. Renwei, Q. Zhenghong, Z. Shuqiao, Experimental research on the dynamic characteristics of the cutting temperature in the process of high-speed milling, Journal of Materials Processing Technology. 138 (2003) 468–471. doi:10.1016/S0924-0136(03)00120-1.

[56] I. Lazoglu, G. Poulachon, C. Ramirez, M. Akmal, B. Marcon, F. Rossi, J. Outeiro, M. Krebs, Thermal analysis in Ti-6Al-4V drilling CIRP Annals 66 (2017) 105-108. doi.org/10.1016/j.cirp.2017.04.020.

[57] R. Komanduri, Z.B. Hou, Thermal modeling of the metal cutting process - Part III: Temperature rise distribution due to the combined effects of shear plane heat source and the tool-chip interface frictional heat source, International Journal of Mechanical Sciences. 43 (2001) 89–107. doi:10.1016/S0020-7403(99)00105-8.

[58] I. Lazoglu, Y. Altintas, Prediction of tool and chip temperature in continuous and interrupted machining, International Journal of Machine Tools and Manufacture. 42 (2002) 1011–1022. doi:10.1016/S0890-6955(02)00039-1.

[59] J.K. Rai, P. Xirouchakis, FEM-based prediction of workpiece transient temperature distribution and deformations during milling, International Journal of Advanced Manufacturing Technology. 42 (2009) 429–449. doi:10.1007/s00170-008-1610-6.

[60] D. Ulutan, I. Lazoglu, C. Dinc, Three-dimensional temperature predictions in machining processes using finite difference method, Journal of Materials Processing Technology. 209 (2009) 1111–1121. doi:10.1016/j.jmatprotec.2008.03.020.

[61] I. Lazoglu, B. Bugdayci, Thermal modelling of end milling, CIRP Annals - Manufacturing Technology. 63 (2014) 113–116. doi:10.1016/j.cirp.2014.03.072.

[62] A. Mamedov, I. Lazoglu, Thermal analysis of micro milling titanium alloy Ti-6Al-4V, Journal of Materials Processing Technology. 229 (2016) 659–667. doi:10.1016/j.jmatprotec.2015.10.019.

[63] Y. Koike, A. Matsubara, I. Yamaji, Design method of material removal process for minimizing workpiece displacement at cutting point, CIRP Annals - Manufacturing Technology. 62 (2013) 419–422. doi:10.1016/j.cirp.2013.03.144.

[64] B. Denkena, D. Boehnke, L. León, Machining induced residual stress in structural aluminum parts, Production Engineering. 2 (2008) 247–253. doi:10.1007/s11740-008-0097-1.

[65] E. Brinksmeier, J. Sölter, Prediction of shape deviations in machining, CIRP Annals - Manufacturing Technology. 58 (2009) 507–510. doi:10.1016/j.cirp.2009.03.123.

[66] I. Lazoglu, D. Ulutan, B.E. Alaca, S. Engin, B. Kaftanoglu, An enhanced analytical model for residual stress prediction in machining, CIRP Annals - Manufacturing Technology. 57 (2008) 81–84. doi:10.1016/j.cirp.2008.03.060.

[67] S. Smith, R. Wilhelm, B. Dutterer, H. Cherukuri, G. Goel, Sacrificial structure preforms for thin part machining, CIRP Annals - Manufacturing Technology. 61 (2012) 379–382. doi:10.1016/j.cirp.2012.03.142.

[68] S. Ratchev, S. Liu, W. Huang, A.A. Becker, Machining simulation and system integration combining FE analysis and cutting mechanics modelling, International Journal of Advanced Manufacturing Technology. 35 (2007) 55–65. doi:10.1007/s00170-006-0700-6.

[69] J.K. Rai, P. Xirouchakis, Finite element method based machining simulation environment for analyzing part errors induced during milling of thin-walled components, International Journal of Machine Tools and Manufacture. 48 (2008) 629–643. doi:10.1016/j.ijmachtools.2007.11.004.

[70] B. Denkena, C. Schmidt, M. Krüger, Experimental investigation and modeling of thermal and mechanical influences on shape deviations in machining structural parts, International Journal of Machine Tools and Manufacture. 50 (2010) 1015–1021. doi:10.1016/j.ijmachtools.2010.06.006.

[71] I. Lazoglu, A. Mamedov, Deformation of thin parts in micromilling, CIRP Annals - Manufacturing Technology. 65 (2016) 117–120. doi:10.1016/j.cirp.2016.04.077.

[72] K. Kothari, R. Radhakrishnan, N.M. Wereley, Advances in gamma titanium aluminides and their manufacturing techniques, Progress in Aerospace Sciences. 55 (2012) 1–16. doi:10.1016/j.paerosci.2012.04.001.

[73] A.L. Mantle, D.K. Aspinwall, Surface integrity and fatigue life of turned gamma titanium aluminide, Journal of Materials Processing Technology. 72 (1997) 413–420. doi:https://doi.org/10.1016/S0924-0136(97)00204-5.

[74] D.K. Aspinwall, R.C. Dewes, A.L. Mantle, The Machining of γ-TiAI Intermetallic Alloys, CIRP Annals. 54 (2005) 99–104. doi:10.1016/S0007-8506(07)60059-6.

[75] R. Hood, P. Cooper, D.K. Aspinwall, S.L. Soo, D.S. Lee, Creep feed grinding of γ-TiAl using single layer electroplated diamond superabrasive wheels, CIRP Journal of Manufacturing Science and Technology. 11 (2015) 36–44. doi:10.1016/j.cirpj.2015.07.001.

[76] A.L. Mantle, D.K. Aspinwall, Surface integrity of a high speed milled gamma titanium aluminide, Journal of Materials Processing Technology. 118 (2001) 143–150. doi:10.1016/S0924-0136(01)00914-1.

[77] P.C. Priarone, S. Rizzuti, L. Settineri, G. Vergnano, Effects of cutting angle, edge preparation, and nano-structured coating on milling performance of a gamma titanium aluminide, Journal of Materials Processing Technology. 212 (2012) 2619–2628. doi:10.1016/j.jmatprotec.2012.07.021.

[78] A. Beranoagirre, D. Olvera, L.N. López De Lacalle, Milling of gamma titanium-aluminum alloys, International Journal of Advanced Manufacturing Technology. 62 (2012) 83–88. doi:10.1007/s00170-011-3812-6.

[79] L. Settineri, P.C. Priarone, M. Arft, D. Lung, T. Stoyanov, An evaluative approach to correlate machinability, microstructures, and material properties of gamma

titanium aluminides, CIRP Annals - Manufacturing Technology. 63 (2014) 57–60. doi:10.1016/j.cirp.2014.03.068.

[80] R. Hood, D.K. Aspinwall, S.L. Soo, A.L. Mantle, D. Novovic, Workpiece surface integrity when slot milling γ-TiAl intermetallic alloy, CIRP Annals - Manufacturing Technology. 63 (2014) 53–56. doi:10.1016/j.cirp.2014.03.071.

[81] J. guang Li, S. qi Wang, Distortion caused by residual stresses in machining aeronautical aluminum alloy parts: recent advances, International Journal of Advanced Manufacturing Technology. 89 (2017) 997–1012. doi:10.1007/s00170-016-9066-6.

[82] Y. Altintas, Manufacturing Automation: Metal Cutting Mechanics, Machine Tool Vibrations, and CNC Design, 2nd ed., Cambridge University Press, Cambridge, 2012. doi:DOI: 10.1017/CBO9780511843723.

[83] L. Lu, J. Sun, K. Guo, J. Li, Study on the Generation and Redistribution Mechanism of Residual Stress in Bilateral Rolling Correction Process for Thin-Walled Parts, ASME 2017 12th International Manufacturing Science and Engineering Conference Collocated with the JSME/ASME 2017 6th International Conference on Materials and Processing. (2017) V001T02A027. doi:10.1115/MSEC2017-2741.

[84] F. Jiang, T. Zhang, L. Yan, Estimation of temperature-dependent heat transfer coefficients in near-dry cutting, International Journal of Advanced Manufacturing Technology. 86 (2016) 1207–1218. doi:10.1007/s00170-015-8293-6.

[85] P. Ii, P. Conditions, M.E. Merchant, Mechanics of the Metal Cutting Orthogonal Cutting, 318 (2004). doi:10.1063/1.1707596.

[86] I.E. Yigit, S.E. Layegh K., I. Lazoglu, A solid modeler based engagement model for 5-axis ball end milling, Procedia CIRP. 31 (2015) 179–184. doi:10.1016/j.procir.2015.03.051.

[87] M. Stanford, P.M. Lister, C. Morgan, K.A. Kibble, Investigation into the use of

gaseous and liquid nitrogen as a cutting fluid when turning BS 970-80A15 (En32b) plain carbon steel using WC-Co uncoated tooling, Journal of Materials Processing Technology. 209 (2009) 961–972. doi:10.1016/j.jmatprotec.2008.03.003.

[88] M. Akmal, K.S.E. Layegh, I. Lazoglu, A. Akgün, Ç. Yavaş, Friction Coefficients on Surface Finish of AlTiN Coated Tools in the Milling of Ti6Al4V, Procedia CIRP. 58 (2017) 596–600. doi:10.1016/j.procir.2017.03.231.